A high-Arctic inner shelf–fjord system from the Last Glacial Maximum to the Present: Bessel Fjord and SW Dove Bugt, NE Greenland

Authors: Kevin Zoller[1]; Jan Sverre Laberg[1]; Tom Arne Rydningen[1], Katrine Husum[2] & Matthias Forwick[1]

[1]Department of Geosciences, UiT The Arctic University of Norway, Box 6050 Langnes, NO-9037 Tromsø, Norway [2]Norwegian Polar Institute, Box 6606 Langnes, NO-9296 Tromsø, Norway

Correspondence to: Kevin Zoller (kevin.zoller3@gmail.com)

Abstract

The Greenland Ice Sheet (GrIS) responds rapidly to the present climate, therefore, its response to the predicted future warming is of concern. To learn more about the impact of future climatic warming on the ice sheet, decoding its behavior during past periods of warmer than present climate is important. However, due to the scarcity of marine studies reconstructing ice sheet conditions on the Northeast Greenland shelf and adjacent fjords, the timing of the deglaciation over marine regions and its connection to forcing factors remain poorly constrained. This includes data collected in fjords that encompass the Holocene Thermal Maximum (HTM), a period in which the climate was warmer than it is at present. This paper aims to use new bathymetric data and the analysis of sediment gravity cores to enhance our understanding of ice dynamics of the GrIS in a fjord and inner shelf environment as well as give insight into the timing of deglaciation and provide a palaeoenvironmental reconstruction of southwestern Dove Bugt and Bessel Fjord since the Last Glacial Maximum (LGM). North-south oriented glacial lineations, and the absence of pronounced moraines in southwest Dove Bugt, an inner continental shelf embayment (trough), suggests the southwards and offshore flow of Storstrømmen, the southern branch of the Northeast Greenland Ice Stream (NEGIS). Sedimentological data suggests that an ice body, theorized to be the NEGIS, may have retreated from the region slightly before ~11.4 cal. ka BP. The seabed morphology of Bessel Fjord, a fjord terminating in southern Dove Bugt, includes numerous basins, separated by thresholds. The position of basin thresholds, which include some recessional moraines, suggest that the GrIS had undergone multiple halts or readvances during deglaciation, likely during one of the cold events identified in the Greenland Summit temperature records. A minimum age of 7.1 cal. ka BP is proposed for the retreat of ice through the fjord to or west of its present-day position in the Bessel Fjord catchment area. This suggests that the GrIS retreated from the marine realm in early Holocene, around the onset of the HTM in this region, a period when the mean July temperature was at least 2-3 °C higher than at present and remained at or west of this onshore position for the remainder of the Holocene. The transition from predominantly mud to muddy sand layers in a mid-fjord core at ~4 cal. ka BP may be the result of increased sediment input from nearby and growing ice caps. This shift may suggest that in the Late Holocene (Meghalayan), a period characterized by a temperature drop to modern values, ice caps in Bessel Fjord probably fluctuated with greater sensitivity to climatic conditions than the NE sector of the GrIS.

# 1. Introduction

Ice mass loss from the Greenland Ice Sheet (GrIS) has accelerated during the 21 century, making it the largest individual contributor to sea level rise (King et al., 2020). This introduction of a substantial quantity of fresh water may have ramifications for global ocean circulations as well as the climate (Rahmstorf et al., 2015). Approximately 12% of the ice from the GrIS is transported to the coast through the Northeast Greenland Ice Stream (NEGIS) (Khan et al., 2014; Joughin et al., 2001) and therefore has a substantial impact on the mass balance of the ice sheet and a potential to contribute to sea level rise. Currently, two of the three marine terminating outlet glaciers that are supplied by the NEGIS are in retreat (Mouginot et al., 2015), where the southernmost branch, Storstrømmen in Dove Bugt (Figs. 1a & 1b), is currently in a building phase following a 1978-1984 surge (Khan et al., 2014; Reeh et al., 1994). While there are numerous studies on the current state of the NEGIS during the past decades to century, there is a scarcity of data concerning the position and dynamics of the ice stream, and other local Northeast Greenland outlet glaciers, on a multi-century to millennia scale over marine regions. Considering that the global mean temperature is expected to continue to rise (Stocker et al., 2013), and that the Arctic will experience an amplification effect (Cohen et al., 2014), looking to the past, especially during warmer than present periods (i.e., the Holocene Thermal Maximum (HTM)), may provide an important insight into the future behavior of the ice sheet.

Marine studies have found evidence for past advancement and retreat of the GrIS and NEGIS along the continental shelf offshore Northeast Greenland (Evans et al., 2009; Winkelmann et al., 2010; Arndt et al., 2015, 2017; Laberg et al., 2017; Arndt, 2018; Olsen et al., 2020; Syring et al., 2020; Davies et al., 2022; Hansen et al., 2022; Jackson et al., 2022). Geomorphological findings in Store Koldewey Trough (~76°N), a major shelf trough northeast of the study area (Fig. 1b), suggests that the ice sheet may have reached the shelf break in this area during the LGM (Last Glacial Maximum) (Laberg et al., 2017; Olsen et al., 2020). However, further north (~79.4°N), findings by Rasmussen et al. (2022) indicate that some regions near the shelf break were ice free during the LGM despite Arndt et al. (2017) positioning the ice front at its maximum LGM position at the outer shelf. A concise understanding of the timing and dynamics of the ice sheet over the NE Greenland shelf during the subsequent deglaciation of the marine realm remains to be established as very few dated cores have been recovered. Terrestrial dating (e.g., cosmogenic nuclide dates and lake studies) has provided further insight into when terrestrial regions had become deglaciated, and how the climate has changed in these areas (e.g., Björck and Persson, 1981; Björck et al., 1994; Wagner et al., 2008; Klug et al., 2009a; Schmidt et al., 2011; Skov et al., 2020; Larsen et al., 2020). However, only recently has terrestrial data been integrated with marine data to establish a detailed deglaciation chronology of the shelf, coastal and fjord regions (Davies et al., 2022; Larsen et al., 2022).

Swath bathymetry and gravity cores data from southwestern Dove Bugt (i.e., Store Bælt) and Bessel Fjord (Fig. 1), presented for the first time in this study, has been used to further refine our understanding of how the GrIS responded to changes in palaeoclimatic conditions from the LGM through the Holocene, including the HTM. Through this analysis we aim to reconstruct regional ice dynamics from both full-glacial conditions and during overall retreat and put our findings into the larger context of the dynamics of the Northeast Greenland Ice Sheet during these periods. Additionally, this study aims to refine our understanding about the timing of deglaciation over marine areas and compare findings to nearby terrestrial regions including the Store Koldewey and Hochstetter Forland/Shannon Ø. Results will also contribute to our

understanding of palaeoenvironmental conditions throughout the Holocene for the NE
88 Greenland fjords and inner shelf areas.
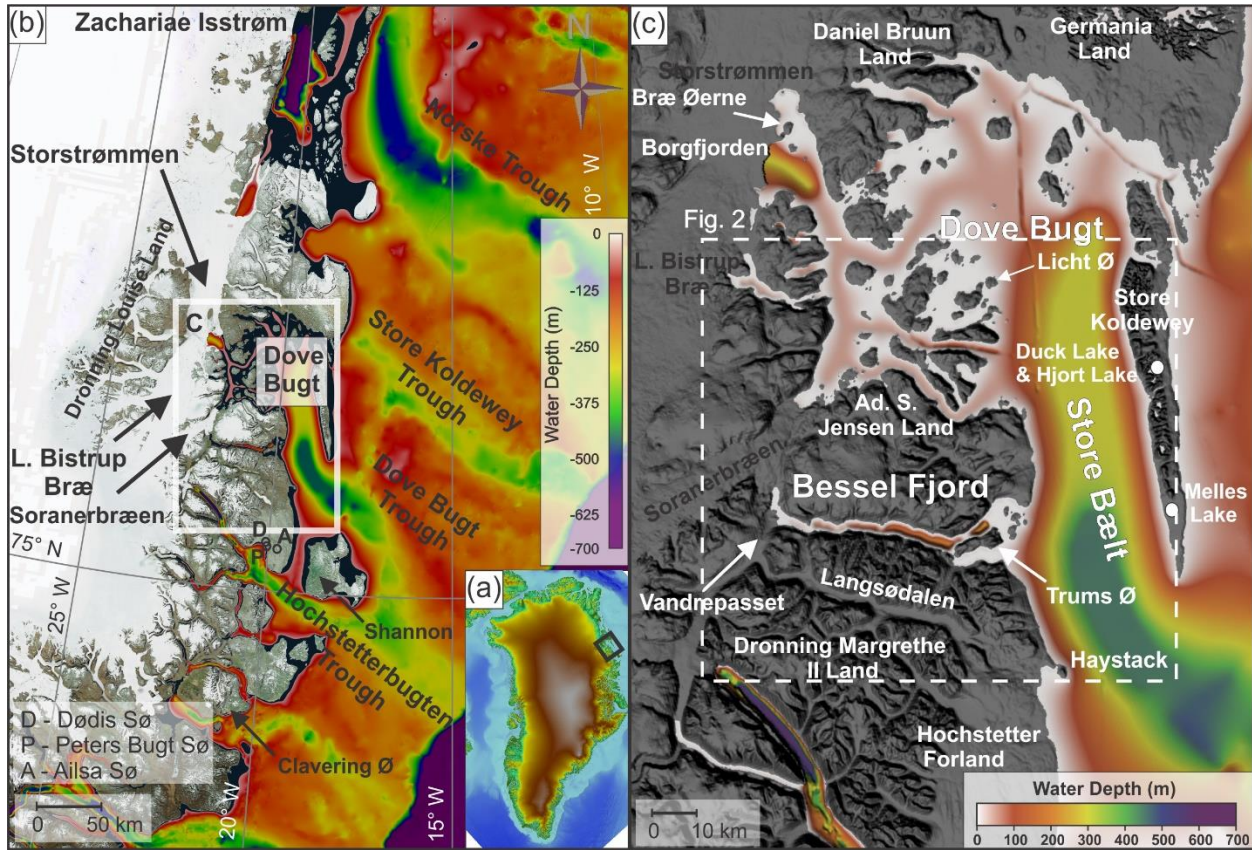
89

90 *Figure 1. (a) An image of Greenland, using IBCAO 4.0 400x400m (Jakobsson et al., 2020), with a black box*
91 *surrounding the study area. (b) Bathymetry of Northeast Greenland displayed using IBCAO 4.0 200x200m data*
92 *(Jakobsson et al., 2020) and land is displayed using a World Imagery satellite image (Earthstar Geographics, Esri,*
93 *HERE, Garmin, FAO, NOAA, USGS) made available through GlobalMapper. The white box surrounds the position of*
94 *Fig. 1c. (c) Bathymetry of Dove Bugt and Bessel Fjord and surrounding land areas displayed using the IBCAO 4.0*
95 *200x200m data (Jakobsson et al., 2020). Locations mentioned in the text are labelled here. The position of Fig. 2 is*
96 *within the white dashed box.*

2. Regional Setting and Environmental History

98 Bessel Fjord is a west-east running fjord between Adolf S. Jensen Land and Dronning
99 Margrethe II Land (Fig. 1c). The western end of the fjord contains the southern outlet glacier
100 Soranerbræen, which also has a second outlet to the north in a tributary fjord to inner Dove Bugt
101 (Fig. 2). Several ice caps are positioned across the length of the fjord (Figs. 2 & 3), some of
102 which have several generations of moraines and glaciofluvial outlets that enter the fjord.
103 Colluvial fans and rivers have been observed across the length of the fjord in satellite images
104 and while surveying the fjord. Multiple islands are located at the entrance of Bessel Fjord, the
105 largest of which, Trums Ø, splits the entrance into two main inlets (Figs. 1c & 2). From the
106 termination of Soranerbræen to the entrance of the fjord measures ~60 km in length. The width
107 of the fjord ranges from 1.8 to 3.7 km.

108 To the west of Bessel Fjord and Soranerbræen is the larger glacier L. Bistrup Bræ, which flows
109 northwards and has an outlet in Borgfjorden, another tributary fjord to inner Dove Bugt (Fig 1).

110 Here it is confluent with the southward flowing NEGIS outlet glacier, Storstrømmen (Rignot et
111 al., 2022). Studies of modern Soranerbræen, L. Bistrup Bræ and Storstrømmen suggest that
112 they all have separate drainage basins (Krieger et al., 2020). Storstrømmen and L. Bistrup Bræ
113 are two of the largest surge-type glaciers in the world (Higgins, 1991) with a surge periodicity of
114 approximately 70 years (Mouginot et al., 2018).

115 Bathymetry of inner Dove Bugt and tributary fjords has revealed that there are no natural large
116 passageways for the warm, salty, subsurface Atlantic Intermediate Water to impact these
117 glaciers at present, therefore it has been suggested that ocean waters do not play a large role in
118 the evolution of Storstrømmen, L. Bistrup Bræ and the northern outlet of Soranerbræen, and
119 that their grounding line retreat is mostly caused by ice thinning (Rignot et al., 2022).

120 Mega-scale glacial lineations (MSGL) identified in Store Koldewey Trough on the continental
121 shelf have been interpreted as evidence for the expanse of this sector of the GrIS to the shelf
122 break during the LGM (Laberg et al., 2017; Olsen et al., 2020). This is further supported by the
123 presence of recessional moraines and grounding zone wedges, which suggests a complex
124 deglaciation of this part of the shelf area (Arndt et al., 2015, 2017; Laberg et al., 2017; Arndt,
125 2018; Olsen et al., 2020). Olsen et al. (2020) has suggested that deglaciation in the Store
126 Koldewey Trough may have occurred in two stages: first, an initial retreat as a result of eustatic
127 sea level rise caused by melting ice at lower latitudes (Lambeck et al., 2014), followed by a
128 melting phase driven by ocean warming. So far, the timing of the onset of the deglaciation is not
129 known. Across the GrIS, deglaciation is believed to be asynchronous, with factors such as
130 topography and local ice dynamics playing a large role with ice retreat in conjunction with
131 climate change (Bennike & Björck, 2002; Funder et al., 2011; Ó Cofaigh et al., 2013; Hogan et
132 al., 2016).

133 A recent study by Jackson et al. (2022) of the inner shelf east of the Clavering Ø (~74°N; Fig.
134 1b) indicated that during the late Younger Dryas, this sector of the GrIS had reached a more
135 landward position, in conformity with Funder et al. (2021). During this period, the inner shelf
136 bottom water was characterized by anomalously high temperatures, interpreted to have played
137 a role in the ice retreat and leading to the termination of the Younger Dryas stadial. This was
138 followed by the onset of the East Greenland Current, as seen from cooler bottom water from the
139 Early Holocene on (Jackson et al., 2022).

140 Further north, east of marine terminating glacier Zachariae Isstrøm (~78° 30N; Fig. 1b), the
141 deglaciation of the NEGIS from the inner shelf was found to have occurred as early as 12.5 cal.
142 ka BP, likely before 13.4 cal. ka BP (Davies et al., 2022). Here, inflow of warmer water (Atlantic
143 Water) may have played a role. This part of the shelf was covered by an ice shelf from 13.4 to
144 11.2 cal. ka BP (including the Younger Dryas), retreating and leading to open water conditions
145 from the earliest Holocene; 11.2-10.8 cal. ka BP, before readvancing from 10.8 to 9.6 cal. ka
146 BP, finally retreating from 9.6 to 7.9 cal. ka BP. At 7.9 cal. ka BP there was a drastic shift in
147 ocean circulation at this site with a sharp decline in Atlantic Water corresponding to an increase
148 in Polar Water influx (Davies et al., 2022). Pados-Dibattista et al. (2022), studying another core
149 from the NE Greenland shelf (more seaward, in a mid-shelf position north of the Norske Trough
150 at ~79°N), found that during the early Holocene (9.4 to 8.2 cal. ka BP), the East Greenland
151 Current was highly stratified with cold surface water overlying warm Atlantic subsurface water.

152
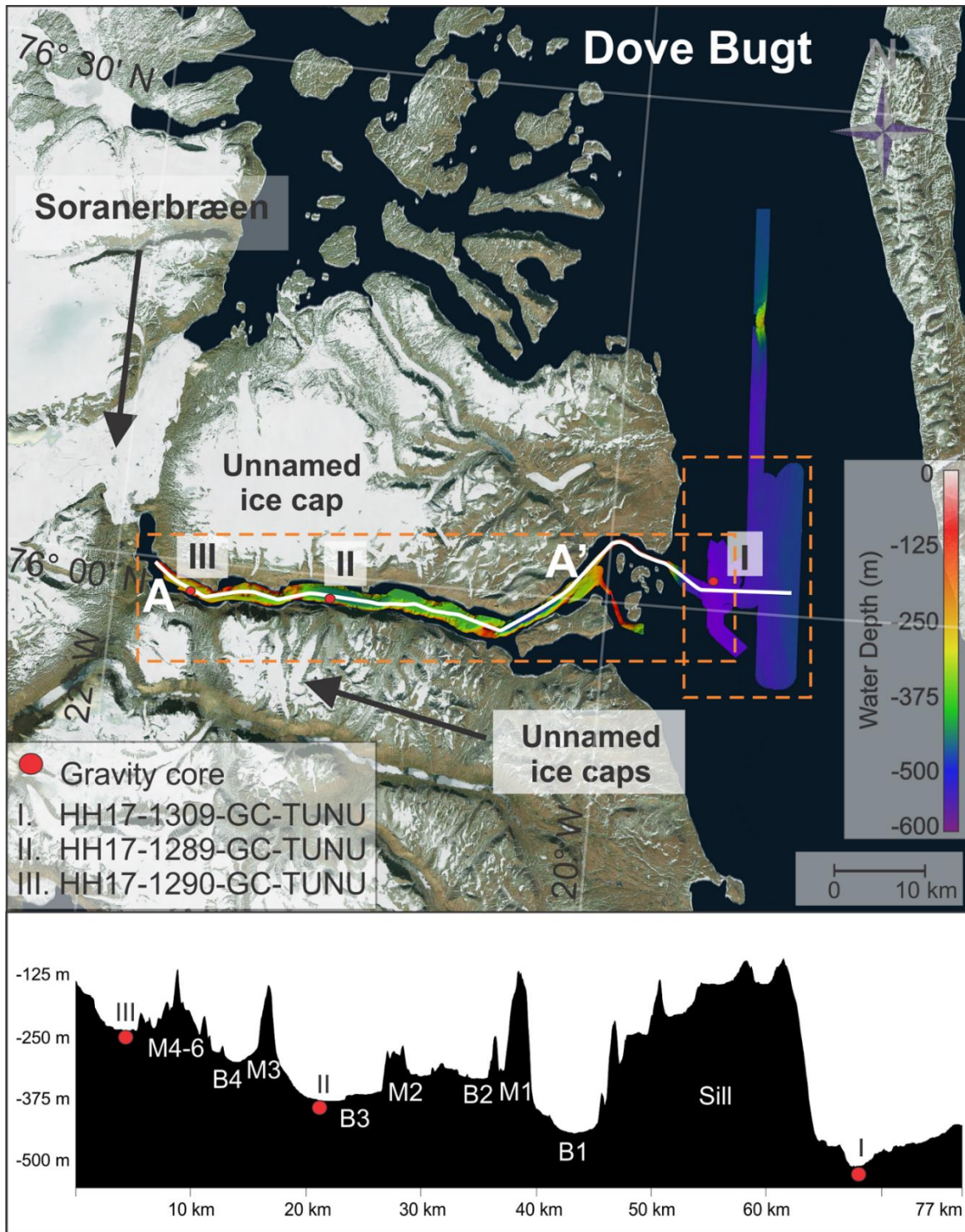
Figure 2. Study area with the bathymetric data showing the locations of the sediment cores presented in this study.
The lower panel is a profile along the length of Bessel Fjord, A-A'. Sediment cores are labelled I, II and III. Satellite
image is displayed using a World Imagery satellite image (Earthstar Geographics, Esri, HERE, Garmin, FAO, NOAA,
USGS) made available through GlobalMapper.

Figure 3. Image of an ice lobe from an ice cap near gravity core HH17-1289-GC-TUNU. Two sets of coarse-grained terminal morainal ridges are indicated by number and arrow. See Fig. 6b for the position of the modern ice lobe. The photograph was taken by Torger Grytå on a 2017 TUNU cruise.

Following the 8.2 ka event, the interval from 8.2 to 6.2 cal. ka BP was followed by the warmest Holocene bottom water conditions on the shelf. Afterwards, conditions returned to those seen prior to 8.2 cal. ka BP due to increased Polar Water transport strengthening the East Greenland Current (Pados-Dibattista et al., 2022).

Terrestrial studies of Dronnings Margrethe II Land, Germania Land and adjacent areas have identified a complex assortment of moraines that are believed to have formed during the Kap Mackenzie, Muschelbjerg, Nanok I and Nanok II stadials (Hjort, 1979, 1981; Hjort and Björck, 1983; Björck et al., 1994; Landvik, 1994). The exact ages of these stadials remain unclear (Table 1), yet Larsen et al. (2022) suggests that Nanok-stadial moraines found in Store Koldewey formed synchronously with the Milne Land moraines of Scoresby Sund which date to the Allerød to early Younger Dryas and Preboreal time (Kelly et al., 2008; Levy et al., 2016).

The position of striations on Store Koldewey and lateral moraines on coastal slopes between Bessel Fjord and Haystack have been interpreted as evidence for ice flowing out of Dove Bugt and Bessel Fjord during the Muschelbjerg stadial, southwards through Store Bælt and turning eastwards around the southernmost mountains of Store Koldewey (Hjort, 1981). Early studies of the region noted glacial and glaciofluvial deposits (e.g., moraine plateau, terminal moraines, eskers and sandurs) on Hochstetter Forland that are believed to have formed during this period (Hjort, 1979, 1981).

Stadials	Studies					Age estimate used in this study
	Hjort & Björck (1983)	Funder et al., (1998)	Kelly et al. (2008)	Vasskog et al. (2015)	Larsen et al. (2022)	
Nanok II	10.1-9.5 cal. ka BP	Preboreal (ending at ca. 9.7 cal. ka BP)	Younger Dryas and Early Holocene (13-11.6 ka (G-III), 11.7-10.6 ka (G II))	Close to Bølling– Allerød transition, and late Younger Dryas (~14 cal. ka BP (G III), ~12 cal. ka BP (G-II))	Preboreal	Preboreal
Nanok I	Older than 14 cal. ka BP, possibly between 15 and 19 cal. ka BP				Late Allerød to early Younger Dryas	Late Allerød to early Younger Dryas
Nanok 0		~48 cal. ka BP (Hjort, unpublished data)				?
Muschelbjerg	Saalian (or older)?					Saalian (or older)?
Kap Mackenzie	Saalian (or older)?					Saalian (or older)?

182

183 Lateral moraines and glacial striations oriented along the axis of Langsodal (also referred to as
184 Langsødalen; Fig. 1c), a nearby valley south of and sub-parallel to Bessel Fjord, have been
185 interpreted as evidence for glacial confinement within the valley during an undifferentiated
186 Nanok stadial (Hjort 1979; Hjort, 1981). This differs from striations that have also been identified
187 in the valley along more weathered surfaces that are oriented in a southwestern direction (Hjort,
188 1979).

189 The outer coastal regions of North and Northeast Greenland are believed to have been
190 deglaciated between 12.8 and 9.7 ka BP and present ice positions were reached between 10.8
191 to 5.8 ka BP (Larsen et al., 2022). Cosmogenic nuclide dates from Store Koldewey, first
192 collected by Håkansson et al. (2007), and later Skov et al. (2020) and Larsen et al. (2022),
193 suggest that ice retreated from the continental shelf and reached the upper and lower sections
194 of the island by 12.3 and 12.7 ka BP, respectively. In contrast, Biette et al. (2020) found
195 evidence of the deglaciation of Clavering Ø at 16.2 ka BP, with readvances at 11.3, 10.8, 3.3,
196 1.2 and 0.37 ka BP. Additional cosmogenic nuclide findings indicate that Trums Ø, in outer

197 Bessel Fjord, may have become deglaciated around 12.6 ka BP and Vandrepasset, onshore
198 inner Bessel Fjord by 8.6 ka BP (Larsen et al., 2022).

199 Findings from macrofossil remains (Bennike & Björck, 2002) and lacustrine sedimentary records
200 (Cremer et al., 2008) suggest that coastal regions were deglaciated in a ~1500 year span after
201 the start of the Holocene (Klug et al., 2016). To the north of Store Koldewey, a minimum date
202 for deglaciation in Germania Land of 9.5 cal. ka BP has been proposed (Landvik, 1994),
203 whereas to the south in southern Dronning Margrethe II Land, a minimum date of 11.2 cal. ka
204 BP has been suggested (Bennike & Weidick, 2001). Lake studies on aquatic organisms at
205 Björck Lake and Hjort Lake on Store Koldewey (Fig. 1c) indicate that the island was at its
206 warmest between ~8 and 4 cal. ka BP, (Wagner et al., 2008; Klug et al., 2009; Schmidt et al.,
207 2011), although findings from Melles Lake (Fig. 1c) suggest that the earliest onset of warmth
208 during the Holocene may have occurred at ~ 10 cal. ka BP (Klug et al., 2009; Briner et al.,
209 2016). On Hochstetter Forland (Fig. 1c), pollen assemblages from Dødis Sø, Peters Bugt Sø
210 and Ailsa Sø suggest that the temperatures were at their highest between 8.8 and 5.6 cal. ka
211 BP (Björck & Persson, 1981; Björck et al., 1994). These findings indicate that the HTM was not
212 uniform across East Greenland, as also described by Briner et al. (2016).

213 To the south, offshore the Kejser Franz Josef Fjord system (~73°N), a detailed biomarker record
214 finds this part of the shelf dominated by seasonal sea ice throughout the Late Holocene (<~5
215 cal. ka BP) and extended concentrations from 5.2 to 2.2 and 1.3 cal. ka BP to present. Short-
216 term variability was also seen for this area for the last 2.2 cal. ka BP, corresponding to the
217 climatic events of this period (Kolling et al., 2017).

218 3. Material and Methods
219 Swath bathymetry and three sediment cores were collected in southwestern Dove Bugt and
220 Bessel Fjord during an expedition aboard RV *Helmer Hanssen* of UiT The Arctic University of
221 Norway in September 2017, being part of the TUNU program (Fig. 2; Christiansen, 2012). The
222 swath bathymetry data was obtained using a Kongsberg Maritime Simrad EM 302 multibeam
223 echo sounder. It was gridded using Petrel software, and geomorphological interpretations were
224 made using Global Mapper 18. Surfaces were developed using a 5x5m grid cell size while a
225 surface created from an International Bathymetric Chart of the Arctic Ocean (IBCAO) dataset
226 4.0 with a 200x200m grid cell size (Jakobsson et al., 2020).

227 Two soft sediment gravity cores were retrieved from Bessel Fjord (HH17-1289-GC-TUNU &
228 HH17-1290-GC-TUNU) and one southwest of Dove Bugt in the sound Store Bælt (HH17-1309-
229 GC-TUNU) (Fig. 2 & Table 2). Prior to splitting the cores, physical properties were measured
230 using a GEOTEK Multi Sensor Core Logger (MSCL-S). The cores were placed in the laboratory
231 for 24 hours prior to obtaining physical measurements to ensure that each core temperature
232 reached equilibrium with the laboratory to avoid distorting p-wave values (Weber et al., 1997).

233 A GEOTEK MSCL X-ray Computed Tomographic imaging machine was also used to scan the
234 unopened core sections to create X-ray radiographic images. After each core was split and
235 cleaned, the characteristics of the sedimentary surface were logged (i.e., structures,
236 bioturbation, grain size, lithological boundaries, etc.), sediment color was noted using the
237 Munsell Soil Color Chart and lithofacies were assigned based on Eyles et al. (1983)
238 classification system. Colored images of the core sections were then obtained using an
239 Avaatech XRF core scanner.

Table 2. Information on the position, water depth and recovery length of each gravity core. Note that the core names
241 *are abbreviated in the text.*

Location	Inner Bessel Fjord	Mid-Bessel Fjord	Southeastern Dove Bugt
Coring station	HH17-1290	HH17-1289	HH17-1309
Latitude [N]	75° 58' 34.5907"	75° 58' 11.4928"	76° 01' 34.0387"
Longitude [W]	21° 07' 13.1055"	21° 41' 48.0278"	19° 34' 31.3190"
Water depth [m]	372	225	512
Recovery [cm]	534.5	245.5	474.55

242

243 Molluscs and benthic foraminifera were recovered from each core for the purpose of
244 radiocarbon dating of lithofacies boundaries. This was, however, not always possible due to the
245 low content of foraminifera and molluscs in these cores which also restricted the number of
246 dates that could be obtained. Two adjacent 1 cm thick sediment slices were successfully
247 sampled from select positions across cores HH17-1290 and HH17-1309. Samples were then
248 wet sieved at 1 mm, 100 µm and 63 µm meshes, respectively. Benthic foraminifera from the
249 100-um size fraction were extracted for radiocarbon dating. Radiocarbon dating was carried out
250 at the MICADAS radiocarbon laboratory at Alfred Wegener Institute, Helmholtz Centre for Polar
251 and Marine Research, Germany. The radiocarbon dates were calibrated using the online
252 version of OxCal 4.4 (https://c14.arch.ox.ac.uk/oxcal.html#program) and the Marine20
253 calibration curve (Heaton et al., 2020), as the calibrated ^{14}C samples are younger than 11.5 cal.
254 ka BP (Heaton et al., 2022). We are using a ΔR of -10 ± 60 in conformity with Jackson et al.
255 (2022). Previously reported radiocarbon dates from this area that are relevant to our study have
256 been recalibrated using Marine20 for marine samples under 11.5 cal. ka BP and IntCal20 for
257 terrestrial samples (Reimer et al., 2020). One marine sample older than 11.5 cal. ka BP has
258 also been included (Table 3). In the Arctic, including our study area, calibration of marine
259 samples by Marine20 is not recommended for samples older than 11.5 cal. ka BP (see Heaton
260 et al. (2022)), therefore, this calibrated age is treated with caution.

261 A Beckman Coulter LS 13 320 Multi-Wavelength Laser Diffraction Particle Size Analyzer was
262 used to perform sediment grain size analysis. Sediment was sampled in mostly 10 cm intervals
263 across HH17-1309, where samples taken from the other two cores were selected from specific
264 positions. Samples were treated in HCl and H_2O_2 and a pre-heated VWB 18 Thermal Bath.
265 Samples were then cleaned using distilled water, placed through multiple runs through a
266 centrifuge and heated in an oven to remove water content. Approximately 0.2 grams of
267 sediment were then separated and placed in a container with 20 ml of water and moved to a
268 shaking table for over 48 hours. A few drops of Calgon were added to each sample, which was
269 then placed into a Branson 200 ultrasonic cleaner for ~7 minutes and shaken briefly before
270 being poured through a >2 mm mesh and into the particle size analyzer. Grains between the
271 size of 0.4 µm and 2000 µm were counted and underwent three separate runs. GRADISTAT
272 Excel-software was used to calculate the mean of the three runs. Sediment names used in
273 reference to this analysis are based on Folk (1954) and mean grain size from the methodology
274 published by Folk & Ward (1957).

275

276

*Table 3. Other published radiocarbon dates and their recalibrated ages using Marine20 (and an ΔR of -10 ± 60 in conformity with Jackson et al. (2022)) and IntCal20 for aquatic moss samples. *The age of sample Lu-1298 from Shannon is above what is recommended by Heaton et al., (2022) for use with Marine20. This date was considered an outlier and therefore not taken into consideration by the authors and Bennike and Björck (2002). Therefore, this date is also rejected in the present study.*

Location	Material	Lab nr.	^{14}C age	^{14}C cal BP (1 σ range)	^{14}C cal BP (median)	Reference
Shannon	shell	Lu-1298*	19000 ± 190	21855-22325	22078	Hjort, 1981; Hjort, 1979
Hochstetter F.	shell	Lu-1289	9190 ± 90	9572-9926	9779	Hjort, 1981; Hjort, 1979
Shannon	shell	Lu-1389	9370 ± 90	9865-10195	10015	Hjort, 1981; Hjort, 1979
Hochstetter F.	shell	Lu-1386	9400 ± 90	9896-10220	10054	Hjort, 1981; Hjort, 1979
Hochstetter F.	shell	Lu-1300:1	9470 ± 90	9970-10322	10157	Hjort, 1981; Hjort, 1979
Hochstetter F.	shell	Lu-1300:2	9520 ± 90	10084-10412	10229	Hjort, 1981; Hjort, 1979
Hochstetter F.	shell	Lu-1384	9810 ± 95	10409-10794	10617	Hjort, 1981; Hjort, 1979
Ardencaple Fjord	shell	Lu-1390	8570 ± 85	8864-9200	9022	Hjort, 1981; Hjort, 1979
Kildedalen	shell	Lu-1303	8930 ± 90	9290-9573	9447	Hjort, 1981; Hjort, 1979
Snenæs	Mya truncata, Hiatella arctica	T-9372	8265 ± 95	8434-8768	8619	Landvik, 1994
Hvalrosodden moraine	Nuculana pernula	TUa-123	8685 ± 95	9006-9315	9166	Landvik, 1994
Hvalrosodden moraine	Nuculana pernula	TUa-124	9045 ± 90	9438-9741	9596	Landvik, 1994
Hvalrosodden	Mya truncata	T-9361	8190 ± 95	8360-8663	8523	Landvik, 1994
Hvalrosodden	Mya truncata, Hiatella arctica	T-9370	7930 ± 120	8681-9085	8890	Landvik, 1994
Hvalrosodden	Mya truncata	T-9371	7490 ± 115	8186-8502	8348	Landvik, 1994
Peters Bugt	Portlandia arctica	Ua-2787	10260 ± 105	11071-11444	11253	Björck et al., 1994
Peters Bugt Sø	Hiatella arctica	Lu-3516	9640 ± 90	10222-10527	10382	Björck et al., 1994
Storstrømmen Sound	Mya truncata & Hiatella arctica	K-6098	5180 ± 95	5220-5520	5352	Weidick et al., 1994
Storstrømmen Sound	Mya truncata	K-5494	4910 ± 85	4865-5175	5028	Weidick et al., 1994
Storstrømmen Sound	Mya truncata	K-5493	4840 ± 90	4793-5117	4943	Weidick et al., 1994
Storstrømmen Sound	Hiatella arctica	Ua-3347	5030 ± 75	5023-5311	5166	Weidick et al., 1994
Storstrømmen Sound	Hiatella arctica	Ua-3350	4180 ± 60	3944-4225	4082	Weidick et al., 1994
Storstrømmen Sound	Balanoptera physalus	K-6096	3630 ± 90	3230-3530	3380	Weidick et al., 1994
Storstrømmen Sound	Hiatella arctica	Ua-3349	3725 ± 60	3371-3616	3496	Weidick et al., 1994
Storstrømmen Sound	Hiatella arctica & Mya truncata	K-6097	3230 ± 85	2749-3024	2897	Weidick et al., 1994
Storstrømmen Sound	Hiatella arctica	Ua-3348	1815 ± 55	1115-1317	1217	Weidick et al., 1994
Hjort Lake	Warnstorfia exannulata	Poz-6194	8260 ± 50	8456-8722	8602	Wagner et al., 2008
Duck Lake	Aquatic moss	LuS-6525	8690 ± 230	9527-10145	9775	Klug et al., 2009

4. Results

4.1. Seafloor landforms in SW Dove Bugt (Store Bælt)

4.1.1. Elongated Lineations - Glacial Lineations

Slightly curved sub-parallel lineations, oriented sub-parallel to the axis of Dove Bugt, are the most pronounced landforms in this part of the study area. They are oriented N-NW in the south and N-NE in the north (Fig. 4). The most frequently identified positive lineations (ridges) are 35-50 m in width, <1-3 m in height and between 1 and 10 km in length. Length to width ratios are frequently >10:1. At elevations shallower than 435 m depth, near the center of Store Bælt, the lineations are wider (e.g., 60-150 m wide), and occasional merging and overlapping of lineations occur (Fig. 4e). Wider lineations, often identified in the southern section of the study area (Fig. 4b), have also been identified with widths, lengths and heights ranging from 200-650 m, 3-8 km, and 4.5-15 m, respectively. Length to width ratios here are 7:1 to >10:1. Some of the larger lineations are superimposed by smaller lineations. Lateral ridges have also been identified in clusters overprinting the lineations (Fig. 4c), where furrows have been found cross cutting lineations (Fig. 4d). Lateral ridges measure 0.5 to 2 m in height and are approximately 45 to 250 m apart.

These elongated lineations are interpreted as glacial lineations (e.g., Ó Cofaigh, 2005). The thinner, more common lineations (with length/width-ratios >10:1) have been interpreted as mega-scale glacial lineations (MSGL), and such landforms are commonly associated with palaeo-ice stream environments (e.g., Stokes & Clark, 2001). Glacial lineations have been identified in numerous continental shelf regions around Greenland (Evans et al., 2009; Dowdeswell et al., 2014; Slabon et al., 2016; Laberg et al., 2017; Newton et al., 2017; Arndt, 2018; Batchelor et al., 2018; Jakobsson et al., 2018). While the mechanism behind the formation of these features are still being debated, some authors have suggested that they may have formed through meltwater flooding (Shaw et al., 2008), groove-ploughing (Clark et al., 2003) or the transverse flow in basal ice (Schoof and Clarke, 2008). King et al. (2009) favored aspects of the dilatant till instability model that could explain the development of MSGLs on a decadal timescale. Sets of ridges that overprint the glacial lineations have been interpreted as recessional moraines, where furrows have been interpreted as iceberg plough marks.

4.1.2. Depression and Mound- Hill-Hole Pair

In northern Store Bælt, a 200 by 450 m wide, 3-4 m deep depression has been identified next to a mound with a width and height of 235 by 450 m and 3-4 m, respectively (Fig. 4d). The depression overprints N-S trending lineations, although the mound contains lineations on its surface.

This depression and mound have been interpreted as a hill-hole pair. These landforms can form when ice-thrust rafts of sediment are removed from the bed by cold-based, slow-flowing ice that transports the sediment that was once in the depression (Hogan et al., 2010; Klages et al., 2013, 2015). In this instance, a south bound ice stream may have removed frozen sedimentary material and deposited it further south. This interpretation is in conformity with studies from other high-latitude continental shelves where subglacial hill-hole pairs are interpreted as formed by ice frozen to the seafloor bed (Sættem, 1990; Ottesen et al., 2005).

328
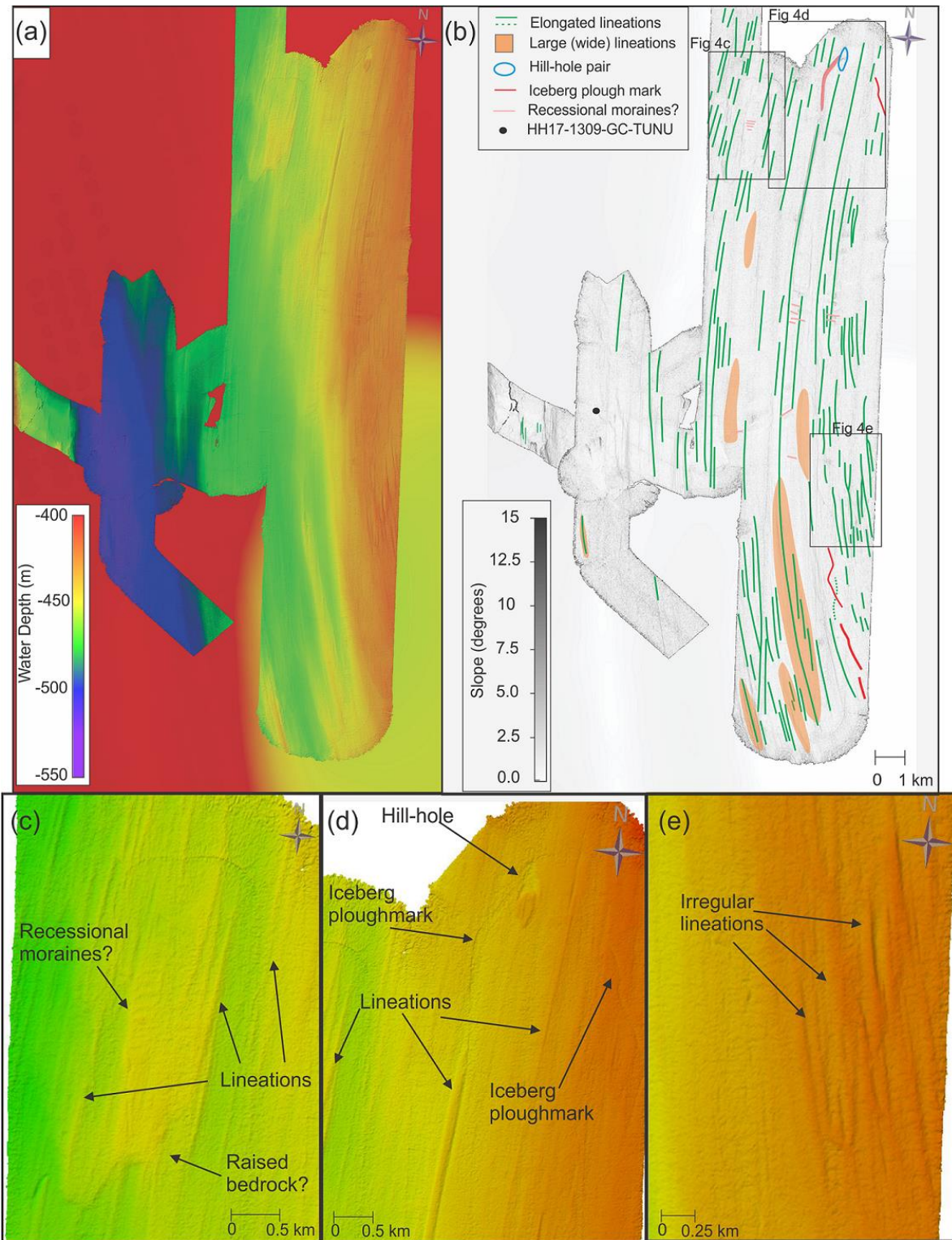
Figure 4. Bathymetric maps from SW Dove Bugt. (a) Seafloor relative to water depth with IBCAO 4.0 displayed in the background (Jakobsson et al., 2020). (b) The main landforms and slope angles of the seafloor in SW Dove Bugt. Locations of Figs. 4c-e are indicated. (c) Bathymetry of the northwestern section of the study area. (d) Bathymetry of the northeaster part of the study area. (e) Bathymetry of the eastern part of the study area showing irregularly shaped glacial lineations.

4.2. Sea floor landforms in Bessel Fjord

4.2.1. Large scale geomorphology

Bessel Fjord contains a variety of basins that are separated by different styles of sills (Figs. 2, 5 & 6). The outermost sill is at the fjord's entrance, and it commonly ranges in depth from 50 to 200 m, with major sections reaching above (and near) the water surface as there are islands in the fjord entrance. Four large basins that are elongated in a west-east direction have been identified in Bessel Fjord (B1-B4). The deepest basin, Basin 1 (B1), is the closest to the fjord entrance and is separated from basin 2 (B2) by a >215 m high sill (M1) that is steeper to the east (Figs. 2 & 5). Basin 3 progressively deepens westwards, with a maximum depth of 380 m. A ~70 to 160 m asymmetrical sill (M3; Figs. 2 & 5) that is steeper on its east side separates Basin 3 from basin 4. Basin 4 is the shallowest basin (~280-300 m) and is adjacent to multiple smaller basins that are primarily at lower points of elevation. The fjord also contains smaller basins that are raised relative to the average seafloor depth (Fig. 6e). Features interpreted as bedrock mounds have also been identified in other sections of the fjord (Figs. 5 & 6). Along the fjord sides, landforms from sediment reworking including slide scars, channels and gullies have also been observed Fig 6b.

4.2.2. Linear Ridges Oriented Along Fjord Axis- Glacial Lineations

Oriented along the fjord's axis (or at times slightly oblique to it), linear features have been identified in the inner and middle of the fjord, as well as a single lineation on the outer part of the fjord (Figs. 5 & 6). They range in size from 100 to 1000 m in length and ~3 to 9 m in height, although some that are as high as 80 m have been identified in the inner fjord. Their morphologies vary throughout the fjord, and their length to width ratios range from 2:1 to 5:1. Most ridges slope towards the outer fjord, although some slope in the opposite direction or have an irregular or flat top. They appear both independently in connection with inferred bedrock highs, and in clusters in flat lying areas of basin 3. These ridges have been interpreted as glacial lineations, and they are thus indicating the direction of former glacier flow.

4.2.3. Transverse Ridges- Moraines

Several transverse ridges have been identified in the inner and central portion of the fjord, oriented perpendicular to the fjord's axis (Figs. 2, 5 & 6). The ridges in the inner most position of the fjord tend to largely conform to the topography (i.e., between bedrock mounds, some of which are position mid-fjord (M4-6; Fig. 6b), and the fjord sidewalls) and are the threshold between sub-basins (Fig. 6). The width and length of ridges range from 150 to 600 m and 120 to 500 m, respectively, where their heights are between <5 to 58 m.

A particularly large, asymmetrical transverse ridge that spans the width of the fjord, is situated between Basin 3 and 4 (M3; Figs. 2 & 6d). This ridge is ~1.5 km in width and between 72 to 162 m in height. It contains a crescent shape in aerial view and is concave towards the mouth of the fjord. A large threshold with a 1.8 km width and a > 215 m height also separates basin 1 and 2 (M1; Figs. 2 & 5). This feature is ~150m shallower in the north and dips steeply into basin 1.

The transverse ridges have been interpreted as moraines, which would have formed during glacial stillstands or readvancements during the retreat of a grounded tidewater glaciers margin. These moraines do not fill the width of the innermost fjord, which has also been seen in inner Nordfjord (part of the Keiser Franz Josef fjord system) by Olsen et al. (2022). While the large transverse ridge M3 is believed to be a moraine, it is considered more likely that M1 is a bedrock mound based on its morphology. The smaller transverse ridges are interpreted as recessional moraines. Smaller moraines have the potential to form at ice margins annually
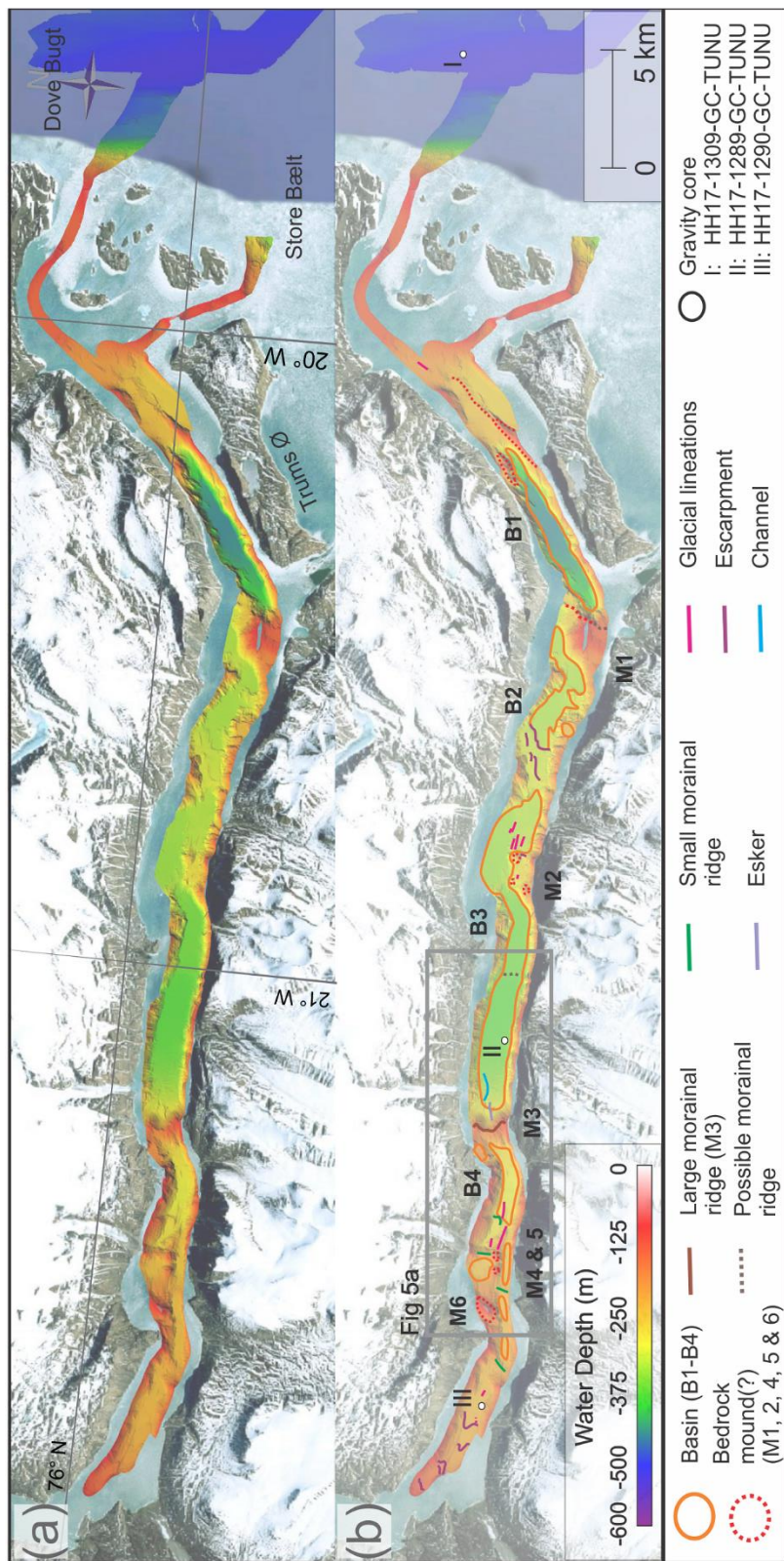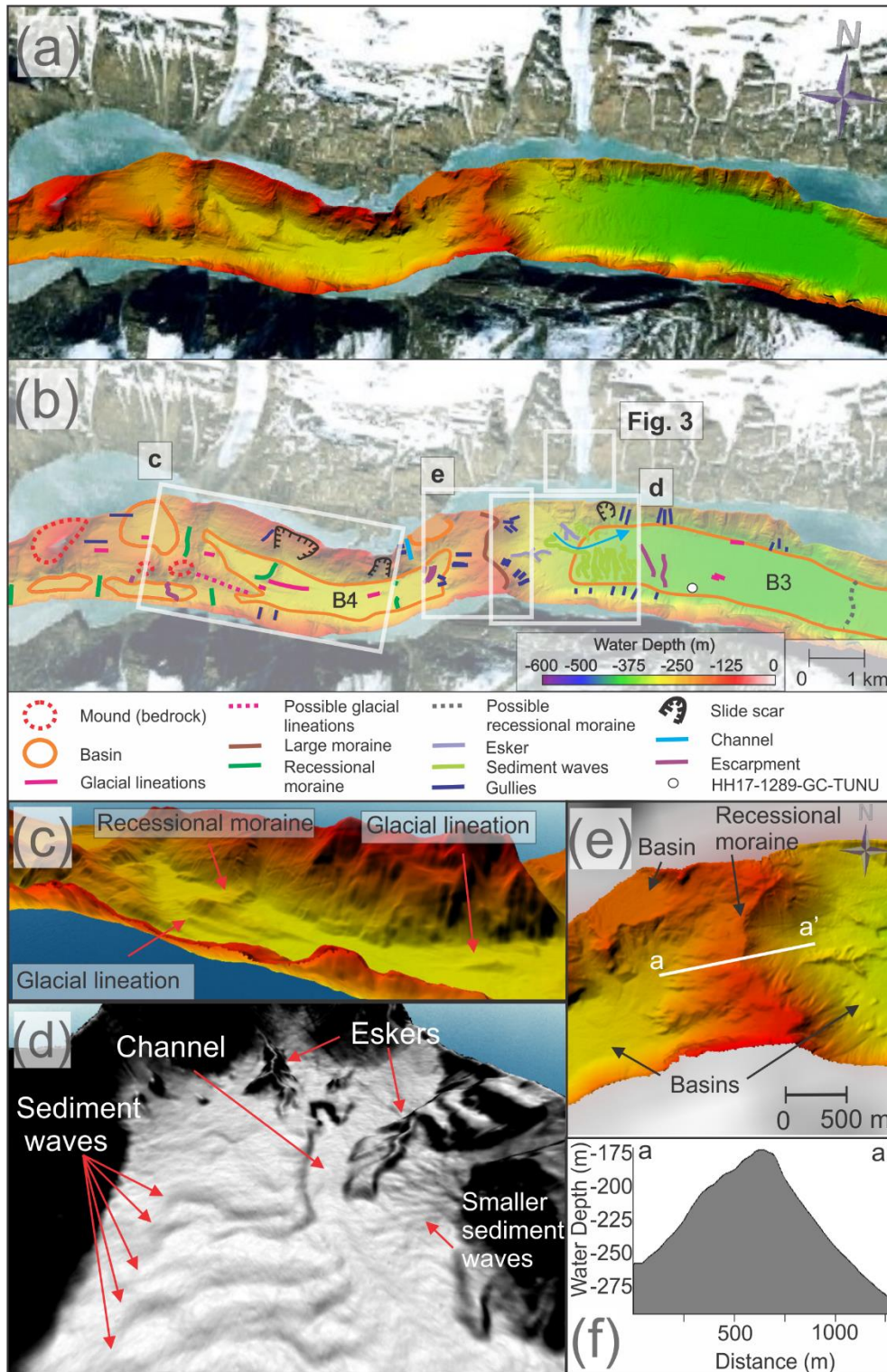
Figure 5. (a) Bathymetric map of Bessel Fjord. (b) A map of mapped features in Bessel Fjord. Satellite images obtained from Google Earth (© Google 2020).

Figure 6. (a-b) Mapped sections from inner to middle Bessel Fjord. Background images used for 6a & 6b obtained from Google Earth (© Google 2020). (c) Glacial lineations in Basin 4 (B4). (d) Eskers, sediment waves and a channel in Basin 3 (B3). (e) A large moraine (M3) between B3 and B4. Note the raised sub-basin to the west and esker to the east. (f) Profile across the large recession moraine (M3).

386　(Lyså & Vorren, 1997; Dowdeswell et al., 2016) and have been observed with a variety of sizes
387　and morphologies on the NE Greenland shelf (e.g., Winkelmann et al., 2010).

4.2.4. Sinuous Ridges- Eskers

389　Sinuous ridges, oriented parallel or oblique to the fjord's axis, occur in basin 3 (Figs. 5, 6b, 6d
390　&6e). These features have widths and lengths of 50 to 120 m, 350 to 800 m, respectively and
391　heights of 10 to 15 m. The most pronounced examples of these ridges have been observed east
392　of the large recessional moraine that has been previously discussed (Fig. 6e).

393　These sinuous ridges have been interpreted as eskers. These landforms form from sediment
394　infill of subglacial and englacial conduits and have been identified in other studies in Greenland
395　(Huddart and Lister, 1981; Geirsdóttir et al., 2000; Winkelmann et al., 2010; Lane et al., 2015).
396　They frequently form in the direction of former ice flow and often form during terminal stages of
397　glaciation, and are therefore associated with moraines (Shreve, 1985). They vary in size
398　depending on the glacial drainage pattern, as well as a number of other factors, however eskers
399　identified within Bessel Fjord appear smaller than those identified in studies in Canada, the UK
400　and Kola Peninsula in Russia (Storrar et al., 2014).

4.2.5. Wavy Transverse Ridges- Sediment Waves

402　Adjacent to the two eskers in Basin 3 are a series of wavy transverse ridges to the east of a
403　large recessional moraine (Figs. 5, 6b & 6d). These features occupy an area of ~500 by 1500 m
404　and contain small ridges and flat areas that slope at an angle of 3 to 6° to the east. Each wave
405　"crest" is ~50 to 100 m apart, although some appear to begin only halfway through the width of
406　the area, where others occupy the entire width, north to south. These waves are crosscut by a
407　channel to the north (Fig. 6d). North of this channel similar features with a wavy morphology
408　occur, although these are substantially smaller.

409　These wavy transverse ridges have been interpreted as sediment waves. Sediment waves
410　found associated with deltaic and glacifluvial deltaic systems have been associated with
411　retrogressive slope failures, gravity-induced sediment creep and/or the migration of sediment
412　waves upslope (Cartigny et al., 2011; Hill, 2012; Stacey and Hill, 2016). Alternatively, given the
413　position of the smaller wavy transverse ridges to the ice cap on Ad. S. Jensen Land (Figs. 1 &
414　2) and the larger ridges to the large moraine to the west (Figs. 5 & 6) it is also possible that
415　these ridges are sets of moraines. Recessional moraines have been identified in the vicinity of
416　eskers in Spitsbergen fjords (Ottesen et al., 2008; Kempf et al., 2013), which may account for
417　the smaller wavy transverse ridges. The larger wavy transverse ridge do also resemble thrust
418　moraines identified by Forwick et al. (2010). Further work may be required in the evaluation of
419　these features. For a full list of observed landforms see Table 4.

4.3. Lithostratigraphy

421　Three gravity cores were retrieved from the study area. Gravity core HH17-1309 was collected
422　in Store Bælt and was sampled from a N/NW-S/SE oriented depression that contains iceberg
423　ploughmarks and a MSGL. Gravity core HH17-1289 was collected in the middle of the Bessel
424　Fjord and is located directly east of the above-mentioned sediment waves on the distal part of
425　the pronounced transverse ridge. Nearby, a modern ice cap fed glacifluvial channel is observed
426　in satellite imagery, likely with a delta at its fjord termination. The gravity core HH17-1290 was
427　collected within the inner fjord, west of the basins and thresholds observed in this study area
428　and is the closest core to Soranerbræen (located ~9.7 km east of the glacier) (Fig. 7).

429

Table 4. Overview of observed landforms in southern Dove Bugt and Bessel Fjord.

Region	Description	Width	Length	Height	Notable Feature	Interpretation
Dove Bugt	Elongated lineations	35-50 m	~1->10 km	<1-3 m	Roughly N-S	Glacial Lineations
	*Wide	200-650 m	3.8 to 8.8. km	4.5-15 m		
	Depression and mound	200 m	450 m	3-4 m	Mound to the south of the depression	Hill-hole pair
	Furrows (scour marks)	~40-100 m	<100-200	3-5 m	Irregular	Iceberg plough marks
	Transverse ridges	150-400 m	~30-100 m	0.5-1 m	Roughly W-E	Recessional moraines
Bessel Fjord	Linear ridge	45-350 m	100-1000 m	3-9, 80 m	Parallel to the fjord's axis	Glacial Lineations
	Transverse ridges	150-600 m	120- 500 m	<5-58 m	Perpendicular to the fjord's axis	Recessional moraines
	*Large ridge (M3)	1485 m	600-1600 m	72 to 162 m		Moraine
	Sinuous ridges	50-120 m	350-800 m	10-15 m		Esker
	Wavy transverse ridges	400-700 m	~45-100 m	2-5 m	Perpendicular to the fjord's axis	Sediment wave
	Elongated depression	~200 m	~1 km	6-8 m		Channels
	Chute	~20-100 m	60-400 m	1-15 m		Gullies

431

### 4.3.1. Facies

Facies 1 – Laminated Mud (Fl, Fl-d & Fl/m-d)

Facies 1 consists of laminated mud (Fl) and laminated mud with dropstones (Fl-d) and have been observed in all three gravity cores (Figs. 7, 8a, 8d & 8f). Laminations are composed of either mud or very fine sand. Mud laminations with finer laminations have also been identified in Unit 3.2 (100-200 cm; Fig. 7a, Fl/m-d). Microfractures have also been identified within this facies (Fig. 8f).

Wet-bulk density measurements tend to increase with depth in some sections of this facies (e.g., 87-350 cm in HH17-1309), suggesting normal sediment consolidation. However, a stagnation or decrease in wet-bulk density with depth in other sections (e.g., below ~350 cm in HH17-1309) suggests less consolidation. The magnetic susceptibility generally tends to increase with depth in HH17-1309 and in Unit 3.2 in HH17-1290, however the remainder of this facies in HH17-1290 (Unit 3.1) remains relatively stable to the base of the core. Notable positive peaks have been identified at 110 and 140 cm in HH17-1309 and measurement fluctuations occur in HH17-1289. Peaks in magnetic susceptibility may reflect the introduction of turbidites or clasts where fluctuations may reflect shifts in sediment provenance.

Muds with sand laminations are believed to have formed through a combination of ice-proximal suspension settling from overflow plumes and turbidity-current activity (underflows). The rhythmically laminated muds are believed to have formed from ice-proximal suspension settling from turbid overflow plumes. Similar laminated sediments have been identified in Kejser Franz Joseph Fjord and Fosters Bugt in East Greenland and are theorized to have been deposited

453
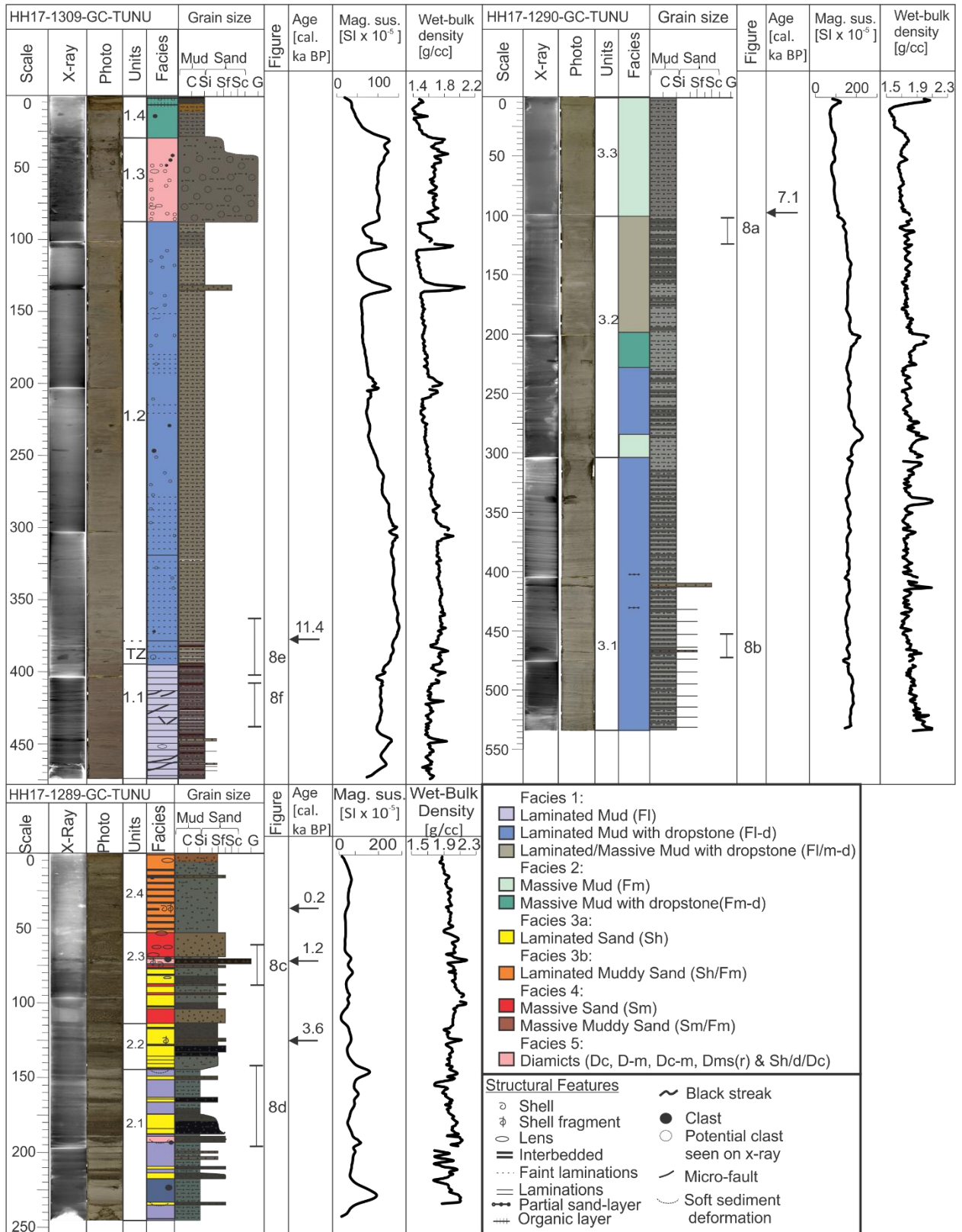
Figure 7. Lithological core logs of the three gravity cores with x-ray images, core photos, unit divisions, facies,
structures, magnetic susceptibility, and wet-bulk density. TZ in HH17-1309-GC-TUNU stands for "Transition Zone".
Grain size abbreviations: C: clay, Si: silt, Sf: fine grained sand, Sc: coarse grained sand and G: gravel.

457
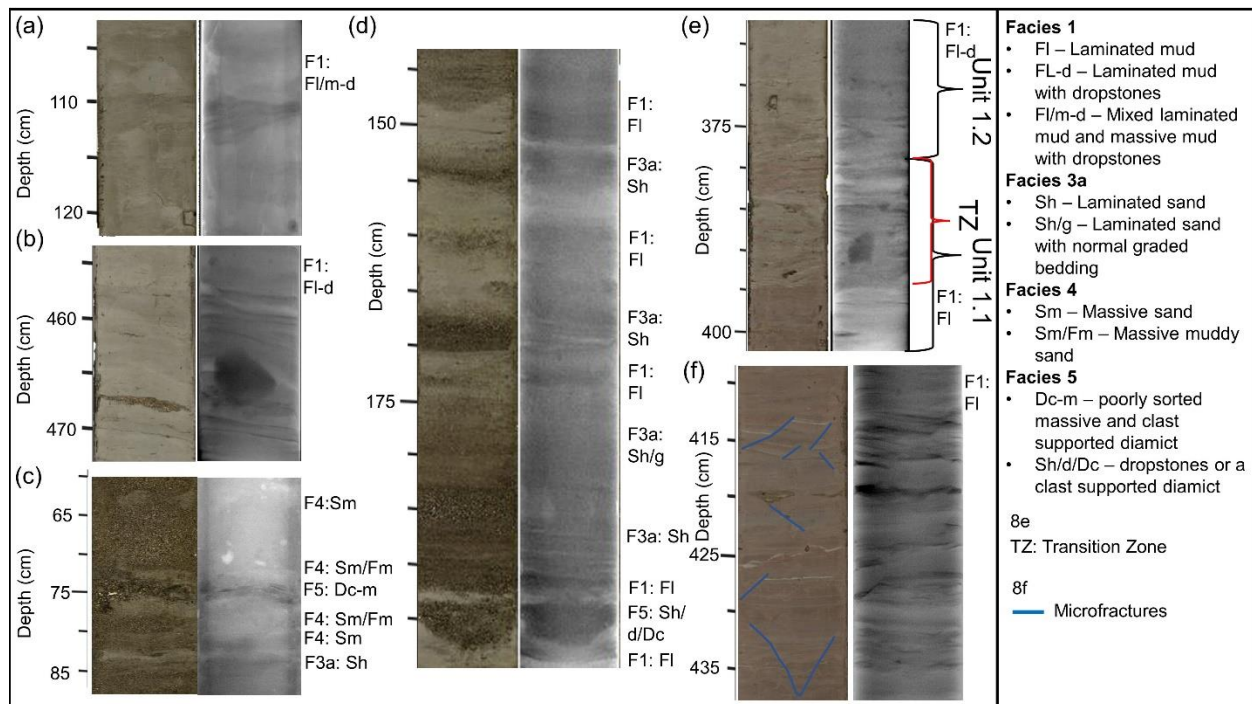
Figure 8. Photographic and x-ray images of sections of the three gravity cores (a-f). Corresponding facies codes can be found to the right of each image.

from turbid meltwater plumes in an ice-proximal environment (Evans et al., 2002). Large clasts have been interpreted as ice rafted debris (IRD). The formation of microfractures may have been caused by soft sediment deformation, possibly from grounded icebergs.

Facies 2 – Massive Mud (Fm & Fm-d)

The second facies consists of massive mud with or without dropstones and can be found in the inner fjord core HH17-1290 and the Store Bælt core HH17-1309 (Fig. 7). In HH17-1290 this appears downcore between sections of Facies 1 as well as in the topmost unit, Unit 3.3. The magnetic susceptibility gradually increases downcore in this facies in Unit 3.3. Further down core, in Unit 3.2, this facies is associated with a downwards trend in magnetic susceptivity following peaks in measured readings. Wet bulk density values roughly mirror these trends. In HH17-1309 massive mud units have been observed in Unit 1.4, where magnetic susceptibility and wet bulk density values increase downcore.

This facies is interpreted as being the result of suspension settling from overflow plumes and is believed to have been deposited in an ice-distal glacimarine environment with varying input from IRD (i.e., Boulton & Deynoux, 1981). Sediment may be sourced from a single location (i.e., Soranerbræen) or more than one location (e.g., local ice caps) in an ice-distal glacimarine environment with limited iceberg or sea-ice rafting. Massive mud deposits have also been identified in other Greenland fjords (e.g., Ó Cofaigh et al., 2001) and it has been suggested that they may indicate meltwater from ice- or fjord margin-distal conditions (Evans et al., 2002).

480 *Facies 3a – Laminated Sand (Sh)*
481 Facies 3a consists of sections of sand with horizontal sand laminations. This facies has been
482 predominantly observed in the mid-fjord core, HH17-1289-GC-TUNU (Figs. 7 & 8d). These
483 sections consist of fine to medium grained sand that range in thickness and colors. Occasionally
484 this facies also contains normal graded bedding (e.g., Fig. 8d, ~174-183 cm). This facies does
485 not contain uniform magnetic susceptibly or wet-bulk density readings as it has been found in
486 association with low and high peaks of both parameters as well as values that are near the
487 average for the core.

488 This facies is interpreted as being deposited from turbidity currents, possibly underflows that are
489 either sourced from glacial or non-glacial streams and slope failures. Uniform layers may
490 indicate a single, rapid event, where shifts in grain size and color may be the result of short-lived
491 fluctuations in sediment input. Laminated sands have been identified in Scoresby Sund in East
492 Greenland and have also been attributed to turbidite formation (Ó Cofaigh et al., 2001).

493 *Facies 3b – Laminated Muddy Sand (Sh/Fm)*
494 Facies 3b represents sections of sand with faint horizontal laminations as well as a large
495 quantity of clay material interspersed throughout with faint laminations. This has been observed
496 in HH17-1289 at the topmost unit in the core, Unit 2.4 (Fig. 7). Magnetic susceptibility is
497 relatively uniform in this facies, where the wet-bulk density tends to decrease up core. Sediment
498 grain size analysis of a single sample from this facies revealed that the sediment is composed
499 of 56.3% sand and 43.7% mud. A "patch" of black organic material (i.e., plant material and
500 shells) was also identified within this unit.

501 This complex facies is believed to have formed predominantly from underflow events, sandy –
502 muddy turbidites, alternatively sandy turbidites with additional input from suspension settling.
503 Similar deposits have been observed in Balsfjord, Norway although without lamination and
504 possibly a higher mud content (Forwick and Vorren, 1998).

505 *Facies 4 – Massive Sand / Massive Muddy Sand (Sm & Sm/Fm)*
506 Facies 4 contains sections of massive sand (Sm) as well as massive sand with a large amount
507 of clay content (Sm/Fm). This facies is predominantly found in Unit 2.3 (and to a much less
508 extent, Unit 2.4) in HH17-1289 (Fig. 7). Sections of massive sand have been found in
509 association with mud lenses and often contain horizontal sand layers (Sh) above and below it.
510 Slight increases and decreases in magnetic susceptibility values have been observed within this
511 facies.

512 This facies is believed to have developed through rapid deposition as well as deformation of
513 Facies 3a & b. According to this interpretation, the mud lenses observed in this facies were
514 once layers/lamina that became deformed due to the sand – mud density contrast. Massive
515 sand has been found in Kangerlussuaq and Miki Fjords in East Greenland (Smith and Andrews,
516 2000) and well-sorted coarse grain deposits have been recovered near Petermann Glacier in
517 northern Greenland (Reilly et al., 2019). Authors have attributed these layers to sediment gravity
518 flows.

519 *Facies 5 – Diamicts (Dc, D-m, Dc-m, Dms(r) & Sh/d/Dc)*
520 Facies 6 contains a variety of different diamicts observed within the mid-fjord core HH17-1289
521 and the Store Bælt core HH17-1309. In HH17-1289 this includes a 3.5 cm poorly sorted
522 massive, and clast supported diamict (Dc-m) in the middle of Unit 2.3 (Figs. 7 & 8c), and a
523 horizontally laminated layer of sand that that is either accompanied by dropstones or a clast

524 supported diamict (Sh/d/Dc) (Figs. 7 & 8d). It is inferred that they are the result of sea ice or
525 iceberg rafting/dumping. Within HH17-1309 there is a substantially larger, sharp based, matrix-
526 supported diamict, stratified in its upper part (Dms(r)) in Unit 1.3 (Fig. 7). Based on these
527 characteristics, this diamict has been interpreted as a density flow deposit, likely a debris flow
528 deposit that is overlain by (part of) a turbidite.

529 *4.3.2. Core chronology*

530 Shell and shell fragments were recovered from HH17-1289 for radiocarbon dating. At 34 cm
531 depth, a semi-spherical path of organic content was identified, containing two intact *Yoldiella*
532 *lenticula*, a shell fragment and plant material. Additionally, at 71 cm depth, a large 3 cm half of a
533 *Hiatella arctica* shell was collected for dating, and shell fragments were recovered from a depth
534 of 125 cm for the same purpose. These shells yielded radiocarbon ages of 0.2, 1.2 and 3.6 cal.
535 ka BP, respectively (Table 5).

536 Cores HH17-1290 and HH17-1309 were subsampled for foraminifera material at four positions
537 and calcareous benthic species were used for dating. In HH17-1290 this included predominantly
538 *Melonis barleeanus* and small amounts of *Islandiella norcrossi*. In HH17-1309, at a depth of 377
539 cm *Islandiella norcrossi* (rare to common), *Stainforthia feylingi* (rare) and a planktonic species
540 were identified immediately above the transition zone between two facies. Radiocarbon dates
541 for the HH17-1309 sample yielded an age of 11.4 cal. ka BP where the sample from HH17-1290
542 yielded an age of 7.1 cal. ka BP (Table 5).

543 *Table 5. Calibrated radiocarbon dates.*

Coring station	Sampling Depth [cm]	Lab nr.	Species	^{14}C age BP	Marine20 cal BP (1σ range)	Marine20 cal BP
HH17-1309-GC-TUNU	377	5157.1.1	Mixed benthic foraminifera	10357 ± 95	11201 - 11553	11386
HH17-1289-GC-TUNU	35	5154.1.1	*Yoldiella lenticula*	688 ± 34	61 - 253	158
HH17-1289-GC-TUNU	71	5155.1.1	*Hiatella arctica*	1747 ± 28	1065 - 1250	1152
HH17-1289-GC-TUNU	125.5	5156.1.1	Bivalve frag.	3809 ± 36	3472 - 3701	3596
HH17-1290-GC-TUNU	97	5158.1.1	Mixed benthic foraminifera	6800 ± 80	6990-7250	7116

544

545

5. Discussion

5.1.   Ice Sheet advance

The appearance of glacial lineations in Bessel Fjord suggest that the fjord was once fully glaciated, which is in accordance with the inferred shelf break-terminating ice sheet inferred for the LGM from other studies (e.g., Laberg et al., 2017; Olsen et al., 2020) (Figs. 9a & 9b). Ice that filled the fjord is believed to most likely be from the modern Soranerbræen glacier but may have also included ice caps and other nearby branches of inland ice.

Glacial lineations are believed to have formed during the LGM but could have also formed during an ice readvance in the deglaciation (see below). Onshore and south of Bessel Fjord, two sets of striations identified in Langsødalen (Hjort, 1979, 1981) may suggest that this valley experienced two glaciation events (Fig. 1c). Striations, and lateral moraines, found along the fjord axis may be the result of the east-west movement of ice through the valley, where SW oriented striations may be the result of Storstrømmen encroaching also onto terrestrial areas. Hjort (1981) suggested that striae on Haystack may indicate that ice flow was dominant from the north during the Nanok Stadial but ice pressure from Langsødalen dominated later after deglaciation begun. Thus, it is possible that ice masses drained through both Bessel Fjord and Langsødalen during full-glacial conditions further advancing into Dove Bugt/Store Bælt.

In Store Bælt, the orientation of glacial lineations (e.g., MSGLs) suggest that ice flowed to the south along the west cost of Store Koldewey, marking the southwards expansion of the Storstrømmen ice stream (Figs. 9a & 9b). East of Dove Bugt, MSGLs identified in Store Koldewey Trough are believed to have formed when the Storstrømmen ice stream acted as a "pure" ice stream (Bentley, 1987; Stokes and Clark, 1999) and overrode the underlying topography during the LGM (Fig. 9a; Olsen et al., 2020). It was theorized that at a later phase, when the ice sheet began to thin, the ice stream became more influenced by the topography of deep troughs, draining northwards to Jøkelbugten and southwards to Dove Bugt (Olsen et al., 2020). Assuming these two phases occurred in the Storstrømmen ice stream development, it is possible that these glacial lineations in Store Bælt represent a period when a branch of the ice stream began conforming to topographical controls (e.g., Store Koldewey) and flowed towards the south. At this point the ice may have flowed into the southeast through Dove Bugt Trough (Fig. 9a).

An alternative interpretation, that cannot be excluded, is that these MSGLs formed during a glacial re-advance that followed the LGM. Between Hochstetter Forland and Shannon Ø a submerged moraine has been identified in Shannon Sound, which may indicate that at one point the ice stream travelled south rather than through Dove Bugt Trough (Figs. 9b & 10a; Hjort, 1981; Landvik, 1994; Larsen et al., 2016; Funder et al., 2021). However, constraints from Store Koldewey, Germania Land and Trums Ø, do not support an ice advance during the Younger Dryas (Fig. 10b; see below). The formation of the submerged moraine was possibly due to an ice readvance of the GrIS outlet(s) (Soranerbræen, L. Bistrup Bræ and/or Storstrømmen) through western, inner Dove Bugt (Fig. 9b), where the surroundings (onshore and offshore) were not or less affected. If this is correct, the readvance may have occurred during the Younger Dryas (prior to 11.4 cal. ka BP, see below).

5.2.   Ice Sheet retreat through Store Bælt

The deglaciation age of 11.4 cal. ka BP (Table 5) from Store Bælt immediately east of the Bessel fjord entrance is attributed to the retreat of a N-S bound branch of the NEGIS (Fig. 9c)
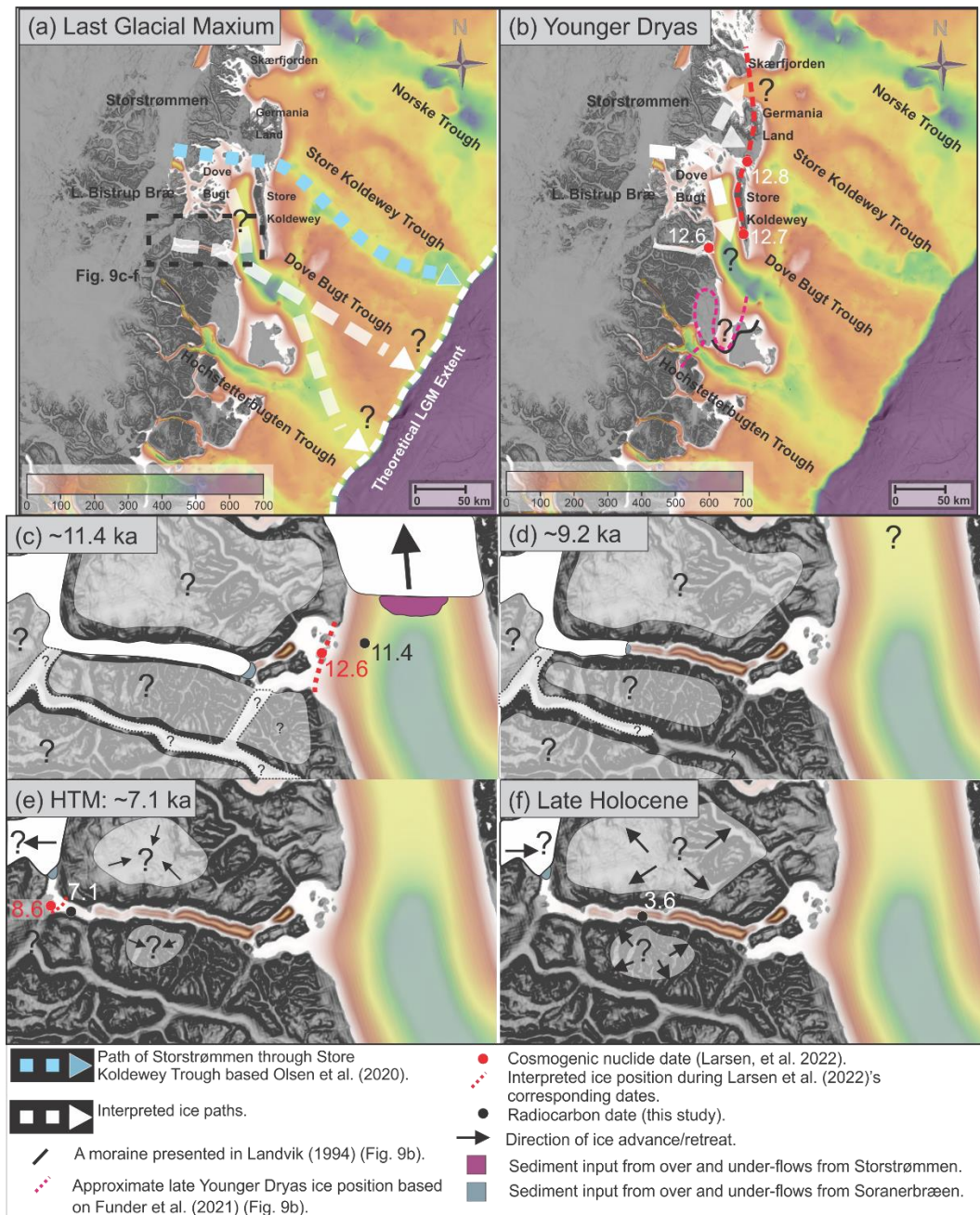
Figure 9. Maps showing ice sheet extent and advancement/retreat directions in SW Dove Bugt and Bessel Fjord during a range of periods. (a) The interpreted position of the ice sheet during the LGM. (b) The theoretical position of ice in Bessel Fjord and Dove Bugt during the Younger Dryas. (c) The ice position in Bessel Fjord at ~11.4 ka based on approximated deglaciation date presented in this study and the position and radiocarbon date for gravity core HH17-1309. The size of ice caps in c-f are only indicative. (d) The position of ice in Bessel Fjord at ~9.2 ka based on approximated deglaciation data from this study. (e) Ice retreating beyond our gravity core (HH17-1290) at ~7.1 ka during the HTM. (f) The Late Holocene ice expanse in Bessel Fjord with a radiocarbon date from gravity core HH17-1289. Background bathymetry displayed using IBCAO data (Jakobsson et al., 2020).

23

599

Figure 10. (a) Marine moraine ridges and glacial lineations from the current study together with previously mapped marine and terrestrial features. (b) Location of deglaciation dates from this study (Table 5) and previous publications. See Table 3 for recalibrated radiocarbon dates. H: Hjort Lake, D: Duck Lake. Background displayed using IBCAO data (Jakobsson et al., 2020).

due to the presence of N-S oriented glacial lineations near the gravity core. This date represents a minimum age for the deglaciation as it is not from the base of the deglacial deposits. Previously published dates constraining the timing of deglaciation in Dove Bugt have been restricted to terrestrial regions (Fig. 10b). Using cosmogenic nuclide dating, Skov et al., (2020) produced deglaciation ages of ca. 12.7 ka at Store Koldewey and ca. 9.8 ka at Pusterdal and later Larsen et al. (2022) produced a number of deglaciation ages across Dove Bugt and Bessel Fjord (8.6-12.8 ka) (Fig. 10b).

Our minimum age of ~11.4 cal. ka BP from HH17-1309 largely matches findings in Dove Bugt and Hochstetter Forland (Fig. 10b). It is slightly later than average cosmogenic nuclide ages obtained from Larsen et al. (2022) on Trums Ø (12.6 ka) and a Nanok moraine on southern Store Koldewey (12.7 ka), but earlier than a second Store Koldewey Nanok moraine (11.0 ka) as well as positions closer to the modern ice margin of Storstrømmen, such as Licht Ø (10.8 ka)

24

617 and Bræ Øerne (8.9 ka). Thus, Store Koldewey, and Trums Ø may have been partially
618 deglaciated slightly prior to the final retreat of the NEGIS through Store Bælt.

619 Radiocarbon dates obtained from lake sediments on Store Koldewey suggest that the earliest
620 onset of warmth may have begun ~10 cal. ka BP (Klug et al., 2009), therefore, the deglaciation
621 of the area beginning prior to this may further support these results. Additionally, Landvik (1994)
622 produced a range of deglaciation ages between 9.6 to 8.5 cal. ka BP along the northern coast of
623 Dove Bugt (Hvalrosodden and Snenæs on Germania Land) and Hjort (1981, 1979) provided a
624 range of delegation ages between 10.6 to 9.8 cal. ka BP on Hochstetter Forland. Later Björck et
625 al. (1994), on Hochstetter Forland, dated *Hiatella arctica* shells near the shore of Peters Bugt
626 Sø and *Portlandia arctica* shells in a delta distal to a Nanok I ridge to 10.4 and 11.3 cal. ka BP,
627 respectively (Table 3; Fig. 10b).

628 Although based on a limited data set, the lack of prominent morainal landforms in Store Bælt
629 may also suggest a rapid retreat through the region. A small number of retreat moraines have
630 been observed in an isolated region of the study area, but the most prominent geomorphic
631 landforms are glacial lineations. Placing Store Bælt within the context of Dowdeswell et al.
632 (2008)'s proposed model for ice streams in high latitudes, ice likely retreated through the area
633 rapidly, although the presence of small moraines may suggest brief periods of stagnation. This
634 is in accordance with findings by Larsen et al. (2020, 2022) that deep fjords and outer regions in
635 eastern North Greenland were rapidly deglaciated between ~12.6 and 10 ka. However,
636 additional data is required to confirm this.

637 Oceanic warming is believed to have contributed to the deglaciation of the inner shelf further
638 north and south of Dove Bugt (e.g., Jackson et al., 2022; Davies et al., 2022). Within the study
639 area, Store Koldewey does largely block oceanic water from the shelf from entering Store Bælt,
640 however, it is possible that warmer water traveled through the Dove Bugt Trough to the south
641 and impacted a north-south branch of the ice stream. This mechanism for warm water transport
642 has also been suggested for other east Greenland troughs (Arndt et al., 2015) and used to
643 explain how warm water has reached other outlets of the NEGIS (e.g., Zachariae Isstrøm via
644 the Norske Trough (Schaffer et al., 2017)).

645 *5.3.   Ice sheet retreat through Bessel Fjord*
646 Cosmogenic nuclide dates from Trums Ø suggest that the deglaciation of the outer fjord began
647 around 12.6 ka (Larsen et al., 2022). Gravity core HH17-1290, collected from the inner fjord
648 region, consists of sediments that reflect an increasingly ice distal environment up core. One
649 radiocarbon date from the core provides a minimum age of ~7.1 cal. ka BP for the deglaciation
650 of Soranerbræen and/or local ice caps from the inner fjord region (Table 5 & Fig. 9e). This date,
651 however, is not from the base of the deglacial deposits and therefore represents a minimum age
652 for the deglaciation of the inner fjord. New cosmogenic nuclide dates from Vandrepasset
653 (onshore innermost Bessel fjord area, connecting the fjord and the next valley to the south)
654 provide an age of 8.6 ka for the deglaciation of the innermost fjord area (Larsen et al., 2022),
655 confirming this interpretation. Our minimum age of 7.1 cal. ka BP and the results of Larsen
656 (2022) falls within a modelled ice sheet extent by Lecavalier et al. (2014) which placed the
657 position of the ice sheet in the middle of Bessel Fjord at 9 cal. ka BP and that the present-day
658 ice margin is reached by 6 cal. ka BP. The minimum age also agrees with the onset of HTM on
659 Store Koldewey (~8.0 to 4.0 cal. ka BP) (Wagner et al., 2008; Klug et al., 2009; Schmidt et al.,
660 2011) and Hochstetter Forland (8.8 and 5.6 cal. ka BP) (Björck & Persson, 1981; Björck et al.,
661 1994). Thus, the GrIS retreated from the marine realm in Early Holocene, slightly before or at

662   the time of the HTM in this region (characterized by a mean July temperature 2-3°C higher than
663   at present; Bennike et al., 2008).

664   The appearance of recessional moraines in Bessel Fjord suggests that the fjord underwent a
665   stepwise deglaciation. The large moraine identified between Basin 3 and Basin 4 (M3; Fig. 7e)
666   is believed to have formed during a major ice halt or readvance, possibly climatically induced.
667   Smaller moraines occasionally follow topographic boundaries, which may suggest that the
668   retreat of ice in Bessel Fjord was also partly topographically controlled. Recessional moraines
669   identied by Olsen et al (2020) east of Dove Bugt in Store Koldewey Trough contain similar
670   heights to those identified here (excluding M3). However, there are more moraines identified in
671   Store Koldwey Trough than in Bessel Fjord, and they are wider, which is likely due to the lack of
672   topographic confinement.

673   A decrease in atmospheric temperatures in early Holocene is recorded in the Greenland
674   Summit temperature records and includes the Preboreal Oscillation and the 9.2 ka event
675   (Kobashi et al., 2017). We tentatively suggest that some of the moraines identified in the Bessel
676   fjord may have developed during some of these events. From this we suggest that increased
677   Northern Hemisphere summer insolation that peaked in the early Holocene was the main
678   control for this part of the deglaciation during which the ice front receded from the coastline to
679   the west of (onshore) Bessel Fjord, a distance of ~60 km. Assuming that this occurred over a
680   maximum period of ~4.3 cal. ka BP (11.4-7.1 cal. ka BP, see discussion above on the timing
681   and length of this period), this corresponds to an average minimum ice recession rate of ~14
682   m/yr. Further supporting this average rate, if one applies this same approach to the two average
683   Bessel Fjord cosmogenic nuclide dates presented by Larsen et al. (2022) (12.6-8.6 ka) and the
684   distance between their sampling locations (~56 km), it also results in a rate of 14 m/yr. This rate
685   is considered realistic as it is half (or less) than the rate estimated from the
686   Nioghalvfjerdsfjorden further north (also part of the Storstrømmen ice stream) where a rate of
687   ~30-40 m/yr was reported (Bennike & Björck, 2002). This rate places Soranerbræen near the
688   large moraine M3 around the 9.2 ka event (Fig. 9d).

689   While oceanic warming may be partially responsible for the retreat of the NEGIS through Store
690   Bælt, we believe that Bessel Fjord is too sheltered by the sill at its entrance to have allowed
691   warm, intermediate water to enter and make a significant impact of the deglaciation of the
692   southern outlet of Soranerbræen. Our bathymetric dataset reveals that the depth of the sill is
693   between ~50 to 200 m, however large parts of it are above water and form islands. This is far
694   shallower than other fjord sills in the region that are theorized to have blocked warm Atlantic
695   Water (e.g., the sill in Dijmphna Sund to the north, which has a maximum depth of 170 m
696   (Wilson and Straneo, 2015)). Also, the effect of the glacio-eustatic readjustment is considered to
697   be small for this region, ~9.5 m higher in the Young Sound region (slightly south of our study
698   area) 7500 years ago (Pedersen et al., 2011). Rignot et al. (2022) also theorized that seafloor
699   topography may impact whether warm water is reaching the northern outlet of Soranerbræen.
700   They suggested further that the grounding line retreat of Storstrømmen, L. Bistrup Bræ, and
701   possibly Soranerbræen, may primarily be caused by ice thinning from atmospheric warming
702   (Rignot et al., 2022). We suggest that a similar mechanism may be responsible for
703   Soranerbræen's retreat through Bessel fjord during the deglaciation.

704   *5.4.   Holocene glacier variability and sedimentary processes in Dove Bugt*
705   Sedimentological evidence (e.g., ice-proximal laminated muds) from HH17-1309 suggests, that
706   suspension settling from a glacial source(s) likely dominated southwestern Dove Bugt during the

Holocene. The contribution of sediment from the NEGIS seems unlikely, as Pusterdal became deglaciated by 9.5 ka (Skov et al., 2020) and Storstrømmen retreated beyond Bræ Øerne by 8.9 ka (Larsen et al., 2022), therefore it very well may be from Soranerbræen, or local ice caps.

During the latter part of the HTM in the middle Holocene, a time period in which some glaciers are believed to have reached their minimum extent across Greenland, the NEGIS is believed to have retreated beyond its current position between 5.4 to 1.2 cal. ka BP (Table 3), creating the Storstrømmen Sound (Weidick et al., 1994). Laminations appear less frequently in the upper part of core HH17-1309, yet they are not absent. Laminations are entirely absent in the Bessel Fjord core HH17-1290 during this period and remain absent through the colder Late Holocene. Later, during the Little Ice Age, Storstrømmen has demonstrated to have expanded to its modern day position (Weidick et al., 1994).

Gravity core HH17-1289, collected to the north of an onshore glaciofluvial channel connected to a modern-day ice cap, transitions to complex assortment of sand layers just prior to 3.6 cal. ka BP (Fig. 7). Sedimentological evidence suggests that these sand layers are largely the result of rapid, short lived depositional events (i.e., turbidity currents) interpreted to be related to the growth of a delta slightly south of the core site, from glaciofluvial sediment input from a nearby outlet glacier.

Pollen assemblage data from Hochstetter Forland mark the end of the HTM at 5.6 cal. ka BP (Björck and Persson, 1981; Björck et al., 1994) and information derived from aquatic organisms mark the end of the HTM on Store Koldewey at 4 cal. ka BP (Wagner et al., 2008; Klug et al., 2009b; Schmidt et al., 2011). This coincides with the onset of turbidites in core HH17-1289. Therefore, it is possible that this shift to sand dominated sedimentation within this core was controlled by climatically driven processes. This onset is here suggested to result from higher sediment input through the channel as local ice caps expanded outwards following the HTM, possibly in response to this climate cooling (Fig. 9f). This period of cooling also corresponds to extended concentrations of sea ice on the shelf (Kolling et al., 2017).

6. Conclusion

In summary:

- Glacial lineations (MSGLs) identified in SW Dove Bugt suggest fast-flowing ice, interpreted to be from the NEGIS, developed during the LGM or an ice readvance during the deglaciation.
- Our minimum deglaciation date for Store Bælt (>11.4 cal. ka BP) is slightly younger than new cosmogenic nuclide dates found onshore on Trums Ø and one of two Nanok stadials on Store Koldewey (Larsen et al., 2022) as well as various other dates across Store Koldewey (e.g., Skov et al., 2020). Thus, Store Koldewey and Trums Ø may have been partially deglaciated prior to the final retreat of the NEGIS through Store Bælt.
- Moraines in Bessel Fjord (to the west of Dove Bugt) suggests that the fjord underwent multiple halts/or readvances upon deglaciation. Thus, the bathymetry of Bessel Fjord indicates that the glacial dynamics of the fjord were more dynamic than onshore evidence suggests.
- The radiocarbon date of 7.1 cal. ka BP obtained in an inner fjord core is interpreted as a minimum age at which Soranerbræen retreated to or beyond its present-day onshore

position west of the fjord and is in conformity with cosmogenic nuclide dates presented by Larsen et al. (2022) in the onshore inner fjord (8.6 ka).

- An average ice recession rate in Bessel Fjord was determined to be ~14 m/yr using data from this study as well as cosmogenic nuclide dates from Larsen et al., (2022).
- The GrIS retreated from the marine realm in the early Holocene, around the time of the onset of the HTM in this region. From this we suggest that increased Northern Hemisphere summer insolation that peaked in the early Holocene was the main control for this part of the deglaciation.
- Sedimentological evidence after 7.1 cal. ka BP in HH17-1289 (i.e., the presence of only massive mud) suggests that Soranerbræen did not expand back into Bessel Fjord for the remainder of the Holocene.
- The transition of mud to muddy sand at 4 cal. ka BP in a mid-fjord core HH17-1289 may provide evidence for local ice cap growth. Thus, ice caps in Bessel Fjord may have fluctuated with greater sensitivity to climatic conditions than the NE sector of the GrIS during the cooling phase that followed the HTM.

References

Arndt, J. E.: Marine geomorphological record of Ice Sheet development in East Greenland since the Last Glacial Maximum, J. Quat. Sci., 33, 853–864, https://doi.org/10.1002/jqs.3065, 2018.

Arndt, J. E., Jokat, W., Dorschel, B., Mykleburst, R., Dowdeswell, J. A., and Evans, J.: A new bathymetry of the Northeast Greenland continental shelf: Constraints on glacial and other processes, AGU Publ. Geochemistry Geophys. Geosystems, 16, 267–300, https://doi.org/10.1002/2014GC005684.Key, 2015.

791 Arndt, J. E., Jokat, W., and Dorschel, B.: The last glaciation and deglaciation of the Northeast
792 Greenland continental shelf revealed by hydro-acoustic data, Quat. Sci. Rev., 160, 45–56, 2017.

793 Batchelor, C. L., Dowdeswell, J. A., and Rignot, E.: Submarine landforms reveal varying rates
794 and styles of deglaciation in North-West Greenland fjords, Mar. Geol., 402, 60–80,
795 https://doi.org/10.1016/j.margeo.2017.08.003, 2018.

796 Bennike, O. and Björck, S.: Chronology of the last recession of the Greenland Ice Sheet, J.
797 Quat. Sci., 17, 211–219, https://doi.org/10.1002/jqs.670, 2002.

798 Bennike, O. and Weidick, A.: Late Quaternary history around Nioghalvfjerdsfjorden and
799 Jøokelbugten, North-East Greenland, Boreas, 30, 205–227, https://doi.org/10.1111/j.1502-
800 3885.2001.tb01223.x, 2001.

801 Bennike, O., Sørensen, M., Fredskild, B., Jacobsen, B. H., BöCher, J., Amsinck, S. L.,
802 Jeppesen, E., Andreasen, C., Christiansen, H. H., and Humlum, O.: Late Quaternary
803 Environmental and Cultural Changes in the Wollaston Forland Region, Northeast Greenland,
804 Adv. Ecol. Res., 40, 45–79, https://doi.org/10.1016/S0065-2504(07)00003-7, 2008.

805 Bentley, C. R.: Antarctic ice streams: a review, Geophys. Res., 92(6), 8843–8858, 1987.

806 Biette, M., Jomelli, V., Chenet, M., Braucher, R., Rinterknecht, V., and Lane, T.: Mountain
807 glacier fluctuations during the Lateglacial and Holocene on Clavering Island (northeastern
808 Greenland) from 10Be moraine dating, Boreas, 49, 873–885, https://doi.org/10.1111/bor.12460,
809 2020.

810 Björck, S. and Persson, T.: Late Weichselian and Flandrian biostratigraphy and chronology from
811 hochstetter forland, northeast Greenland, Medd. Om. Grønl. Geosci., 5, 1–19, 1981.

812 Björck, S., Wohlfarth, B., Bennike, O., Hjort, C., and Persson, T.: Revision of the early Holocene
813 lake sediment based chronology and event stratigraphy on Hochstetter Forland, NE Greenland,
814 Boreas, 23, 513–523, https://doi.org/10.1111/j.1502-3885.1994.tb00619.x, 1994.

815 Boulton, G. S. and Deynoux, M.: Sedimentation in glacial environments and the identification of
816 tills and tillites in ancient sedimentary sequences, Precambrian Res., 15, 397–422,
817 https://doi.org/10.1016/0301-9268(81)90059-0, 1981.

818 Boulton, G. S., Hagdorn, M., and Hulton, N. R. J.: Streaming flow in an ice sheet through a
819 glacial cycle, Ann. Glaciol., 36, 117–128, https://doi.org/10.3189/172756403781816293, 2003.

820 Briner, J. P., McKay, N. P., Axford, Y., Bennike, O., Bradley, R. S., de Vernal, A., Fisher, D.,
821 Francus, P., Fréchette, B., Gajewski, K., Jennings, A., Kaufman, D. S., Miller, G., Rouston, C.,
822 and Wagner, B.: Holocene climate change in Arctic Canada and Greenland, Quat. Sci. Rev.,
823 147, 340–364, https://doi.org/10.1016/j.quascirev.2016.02.010, 2016.

824 Cartigny, M. J. B., Postma, G., Berg, J. H., and Mastbergen, D. R.: A comparative study of
825 sediment waves and cyclic steps based on geometries, internal structures and numerical
826 modeling, Mar. Geol., 280, 40–56, 2011.

827 Christiansen, J. S.: The TUNU-Programme : Euro-Arctic Marine Fishes — Diversity and
828 Adaptation, in: Adaptation and Evolution in Marine Environments, vol. 1, 35–50,
829 https://doi.org/10.1007/978-3-642-27352-0, 2012.

830 Clark, C. D.: Mega-scale lineations and cross-cutting ice-flow landforms, Earth Surf. Process.
831 Landforms, 18, 1–29, 1993.

832 Clark, C. D. and Stokes, C. R.: Palaeo-ice stream landsystem, in: Glacial Landscapes, edited
833 by: Evans, D. J. A., Edward Arnold, London, 204–227, 2003.

834 Clark, C. D., Tulaczyk, S. M., Stokes, C. R., and Canals, M.: A groove-ploughing theory for the
835 production of mega-scale glacial lineations, and implications for ice-stream mechanics, J.
836 Glaciol., 49, 240–256, https://doi.org/10.3189/172756503781830719, 2003.

837 Cohen, J., Screen, J. A., Furtado, J. C., Barlow, M., Whittleston, D., Coumou, D., Francis, J.,
838 Dethloff, K., Entekhabi, D., Overland, J., and Jones, J.: Recent Arctic amplification and extreme
839 mid-latitude weather, Nat. Publ. Gr., 7, 627–637, https://doi.org/10.1038/ngeo2234, 2014.

840 Cremer, H., Bennike, O., and Wagner, B.: Lake sediment evidence for the last deglaciation of
841 eastern Greenland, Quat. Sci. Rev., 27, 312–319,
842 https://doi.org/10.1016/j.quascirev.2007.09.004, 2008.

843 Davies, J., Mathiasen, A. M., Kristiansen, K., Hansen, K. E., Wacker, L., Alstrup, A. K. O., Munk,
844 O. L., Pearce, C., and Seidenkrantz, M. S.: Linkages between ocean circulation and the
845 Northeast Greenland Ice Stream in the Early Holocene, Quat. Sci. Rev., 286, 107530,
846 https://doi.org/10.1016/j.quascirev.2022.107530, 2022.

847 Dowdeswell, J. A., Ottesen, D., Evans, J., Cofaigh, C. Ó., and Anderson, J. B.: Submarine
848 glacial landforms and rates of ice-stream collapse, Geology, 36, 819–822,
849 https://doi.org/10.1130/G24808A.1, 2008.

850 Dowdeswell, J. A., Hogan, K. A., Ó Cofaigh, C., Fugelli, E. M. G., Evans, J., and Noormets, R.:
851 Late Quaternary ice flow in a West Greenland fjord and cross-shelf trough system: submarine
852 landforms from Rink Isbrae to Uummannaq shelf and slope, Quat. Sci. Rev., 92, 292–309,
853 2014.

854 Dowdeswell, J. A., Canals, M., Jakobsson, M., Todd, B. J., Dowdeswell, E. K., and Hogan, K.
855 A.: The variety and distribution of submarine glacial landforms and implications for ice-sheet
856 reconstruction, Geol. Soc. Mem., 46, 519–552, https://doi.org/10.1144/M46.183, 2016.

857 Evans, J., Dowdeswell, J. A., Grobe, H., Niessen, F., Stein, R., Hubberten, H. W., and
858 Whittington, R. J.: Late Quaternary sedimentation in Kejser Franz Joseph Fjord and the
859 continental margin of East Greenland, Geol. Soc. Spec. Publ., 203, 149–179,
860 https://doi.org/10.1144/GSL.SP.2002.203.01.09, 2002.

861 Evans, J., Ó Cofaigh, C., Dowdeswell, J. A., and Wadhams, P.: Marine geophysical evidence
862 for former expansion and flow of the Greenland Ice Sheet across the north-east Greenland
863 continental shelf, J. Quat. Sci., 24, 279–293, 2009.

864 Eyles, N., Eyles, C. H., and Niall, An. D.: Lithofacies types and vertical profile models; an
865 alternative approach to the description and environmental interpretation of glacial diamict and
866 diamictite sequences, Sedimentology, 30, 393–410, 1983.

867 Folk, R. L.: The Distinction between Grain Size and Mineral Composition in Sedimentary-Rock
868 Nomenclature, J. Geol., 62, 344–359, 1954.

869 Folk, R. L. and Ward, W.: Brazos river bar, a study in the significance of grain size parameters.,
870 J. Sediment. Petrol., 27, 34–59, 1957.

871 Forwick, M. and Vorren, T. O.: Deglaciation history and post-glacial mass movements in
872 Balsfjord, northern Norway, Polar Res., 21(2), 259–266, 1998.

873 Forwick, M., Vorren, T. O., Hald, M., Korsun, S., Roh, Y., Vogt, C., and Yoo, K. C.: Spatial and

874   temporal influence of glaciers and rivers on the sedimentary environment in Sassenfjorden and
875   Tempelfjorden, Spitsbergen, Geol. Soc. London, Spec. Publ., 344, 163–193,
876   https://doi.org/10.1144/SP344.13, 2010.

877   Funder, S., Kjeldsen, K. K., Kjær, H. K., and Ó Cofaigh, C.: The Greenland Ice Sheet During the
878   Past 300,000 Years: A Review, Dev. Quat. Sci., 15, 699–713, https://doi.org/10.1016/B978-0-
879   444-53447-7.00050-7, 2011.

880   Funder, S., Sørensen, A. H. L., Larsen, N. K., Bjørk, A. A., Briner, J. P., Olsen, J., Schomacker,
881   A., Levy, L. B., and Kjær, K. H.: Younger Dryas ice margin retreat in Greenland: new evidence
882   from southwestern Greenland, Clim. Past, 17, 587–601, 2021.

883   Geirsdóttir, Á., Hardardóttir, J., and Andrews, J. T.: Late-Holocene terrestrial glacial history of
884   Miki and I.C. Jacobsen Fjords, East Greenland, Holocene, 10, 123–134,
885   https://doi.org/10.1191/095968300666213169, 2000.

886   Håkansson, L., Graf, A., Strasky, S., Ivy-ochs, S., Kubik, P. W., Hjort, C., Shlüchter, C.,
887   Geografiska, S., Series, A., Geography, P., Hakansson, L., Graf, A., Strasky, S., Ivy-ochs, S.,
888   Kubik, P. W., Hjort, C., and Schlichter, C.: Cosmogenic 10Be-Ages from the Store Koldewey
889   Island, NE Greenland, Geogr. Ann. Ser. A Phys. Geogr., 89, 195–202, 2007.

890   Hansen, K. E., Lorenzen, J., Davies, J., Wacker, L., Pearce, C., and Seidenkrantz, M.-S.:
891   Deglacial to Mid Holocene environmental conditions on the northeastern Greenland shelf,
892   Quanternary Sci. Rev., 293, 107704, 2022.

893   Heaton, T. J., Köhler, P., Butzin, M., Bard, E., Reimer, R. W., Austin, W. E. N., Ramsey, C. B.,
894   Grootes, P. M., Hughen, K. A., Kromer, B., Reimer, P. J., and Heaton, T. J.: Marine20 — The
895   Marine Radiocarbon Age Calibration Curve (0-55,000 CAL BP), Radio, 62, 779–820,
896   https://doi.org/10.1017/RDC.2020.68, 2020.

897   Heaton, T. J., Bard, E., Ramsey, C. B., Butzin, M., Hatté, C., Hughen, K. A., Köhler, P., and
898   Reimer, P. J.: A Response to Community Questions on the Marine20 Radiocarbon Age
899   Calibration Curve: Marine Reservoir Ages and The Calibration of 14C Samples from the
900   Oceans, Radiocarbon, 65, 247–273, https://doi.org/10.1017/RDC.2022.66, 2022.

901   Higgins, A. K.: North Greenland Glaeier Velocities and Calf Ice Production, Polarforschung, 60,
902   1–23, 1991.

903   Hill, P. R.: Changes in submarine channel morphology and strata development from repeat
904   multibeam surveys in the Fraser River delta, western Canada, in: Sediments, Morphology and
905   Sedimentary Processes on Continental Shelves, edited by: Li, M. Z., Sherwood, C. R., and Hill,
906   P. R., Blackwell Science, International Association of Sedimentologists, 47–70, 2012.

907   Hjort, C.: Glaciation in northern East Greenland during the Late Weichselian and Early
908   Flandrian, Boreas, 8, 281–296, https://doi.org/10.1111/j.1502-3885.1979.tb00812.x, 1979.

909   Hjort, C.: A glacial chronology for northern East Greenland, Boreas, 10, 259–274, 1981.

910   Hjort, C. and Björck, S.: A re-evaluated glacial chronology for Northern East Greenland, Geol.
911   Föreningen i Stock. Förhandlingar, 105, 235–243, https://doi.org/10.1080/11035898309452590,
912   1983.

913   Hogan, K. A., Dowdeswell, J. A., Noormets, R., Evans, J., and Ó Cofaigh, C.: Evidence for full-
914   glacial flow and retreat of the Late Weichselian Ice Sheet from the waters around Kong Karls
915   Land, eastern Svalbard, Quat. Sci. Rev., 29, 3563–3582,
916   https://doi.org/10.1016/j.quascirev.2010.05.026, 2010.

Hogan, K. A., Ó Cofaigh, C., Jennings, A. E., Dowdeswell, J. A., and Hiemstra, J. F.: Deglaciation of a major palaeo-ice stream in Disko Trough, West Greenland, Quat. Sci. Rev., 147, 5–26, 2016.

Huddart, D. and Lister, H.: The Origin of Ice Marginal Terraces and Contact Ridges of East Kangerdluarssuk Glacier, SW Greenland, Geogr. Ann., 63 A, 31–39, 1981.

Jackson, R., Andreasen, N., Oksman, M., Andersen, T. J., Pearce, C., Seidenkrantz, M.-S., and Ribeiro, S.: Marine conditions and development of the Sirius Water polynya on the North-East Greenland shelf during the Younger Dryas-Holocene, Quat. Sci. Rev., 291, 107647, 2022.

Jakobsson, M., Hogan, K. A., Mayer, L. A., Mix, A., Jennings, A., Stoner, J., Eriksson, B., Jerram, K., Mohammad, R., Pearce, C., Reilly, B., and Stranne, C.: The Holocene retreat dynamics and stability of Petermann Glacier in northwest Greenland, Nat. Commun., 9, https://doi.org/10.1038/s41467-018-04573-2, 2018.

Jakobsson, M., Mayer, L. A., Bringensparr, C., Castro, C. F., Mohammad, R., Johnson, P., Ketter, T., Accettella, D., Amblas, D., An, L., Arndt, J. E., Canals, M., Casamor, J. L., Chauché, N., Coakley, B., Danielson, S., Demarte, M., Dickson, M. L., Dorschel, B., Dowdeswell, J. A., Dreutter, S., Fremand, A. C., Gallant, D., Hall, J. K., Hehemann, L., Hodnesdal, H., Hong, J., Ivaldi, R., Kane, E., Klaucke, I., Krawczyk, D. W., Kristoffersen, Y., Kuipers, B. R., Millan, R., Masetti, G., Morlighem, M., Noormets, R., Prescott, M. M., Rebesco, M., Rignot, E., Semiletov, I., Tate, A. J., Travaglini, P., Velicogna, I., Weatherall, P., Weinrebe, W., Willis, J. K., Wood, M., Zarayskaya, Y., Zhang, T., Zimmermann, M., and Zinglersen, K. B.: The International Bathymetric Chart of the Arctic Ocean Version 4.0, Sci. Data, 7, 1–14, https://doi.org/10.1038/s41597-020-0520-9, 2020.

Joughin, I., Fahnestock, M., MacAyeal, D., Bamber, J. L., and Gogineni, P.: Observation and analysis of ice flow in the largest Greenland ice stream, J. Geophys. Res. Atmos., 106, 34021–34034, https://doi.org/10.1029/2001JD900087, 2001.

Kelly, M. A., Lowell, T. V., Hall, B. L., Schaefer, J. M., Finkel, R. C., Goehring, B. M., Alley, R. B., and Denton, G. H.: A 10Be chronology of lateglacial and Holocene mountain glaciation in the Scoresby Sund region, east Greenland: implications for seasonality during lateglacial time, Quat. Sci. Rev., 27, 2273–2282, 2008.

Kempf, P., Forwick, M., Laberg, J. S., and Vorren, T. O.: Late Weichselian and Holocene sedimentary palaeoenvironment and glacial activity in the high-arctic van Keulenfjorden, Spitsbergen, The Holocene, 23 (11), 1607–1618, https://doi.org/10.1177/0959683613499055, 2013.

Khan, S. A., Kjær, K. H., Bevis, M., Bamber, J. L., Wahr, J., Kjeldsen, K. K., Bjørk, A. A., Korsgaard, N. J., Stearns, L. A., Van Den Broeke, M. R., Liu, L., Larsen, N. K., and Muresan, I. S.: Sustained mass loss of the northeast Greenland ice sheet triggered by regional warming, Nat. Clim. Chang., 4, 292–299, https://doi.org/10.1038/nclimate2161, 2014.

King, E. C., Hindmarsh, R. C. A., and Stokes, C. R.: Formation of mega-scale glacial lineations observed beneath a West Antarctic ice stream, Nat. Geosci., 2, 585–588, https://doi.org/10.1038/ngeo581, 2009.

King, M. D., Howat, I. M., Candela, S. G., Noh, M. J., Jeong, S., Noël, B. P. Y., van den Broeke, M. R., Wouters, B., and Negrete, A.: Dynamic ice loss from the Greenland Ice Sheet driven by sustained glacier retreat, Commun. Earth Environ., 1, 1–7, https://doi.org/10.1038/s43247-020-0001-2, 2020.

Klages, J. P., Kuhn, G., Hillenbrand, C.-D., Graham, A. G. C., Smith, J. A., Larter, R. D., and Gohl, K.: First geomorphological record and glacial history of an inter-ice stream ridge on the West Antarctic continental shelf, Quat. Sci. Rev., 61, 47–61, 2013.

Klages, J. P., Kuhn, G., Graham, A. G. C., Hillenbrand, C.-D., Smith, J. A., Nitsche, F. O., Larter, R. D., and Gohl, K.: Palaeo-ice stream pathways and retreat style in the easternmost Amundsen Sea Embayment, West Antarctica, revealed by combined multibeam bathymetric and seismic data, Geomorphology, 245, 207–222, 2015.

Klug, M., Schmidt, S., Melles, M., Wagner, B., Bennike, O., and Heiri, O.: Lake sediments from Store Koldewey, Northeast Greenland, as archive of Late Pleistocene and Holocene climatic and environmental changes, Boreas, 38, 59–71, https://doi.org/10.1111/j.1502-3885.2008.00038.x, 2009a.

Klug, M., Bennike, O., and Wagner, B.: Repeated short-term bioproductivity changes in a coastal lake on Store Koldewey, northeast Greenland: An indicator of varying sea-ice coverage?, Holocene, 19, 653–663, https://doi.org/10.1177/0959683609104040, 2009b.

Klug, M., Bennike, O., and Wagner, B.: Late Pleistocene to early Holocene environmental changes on Store Koldewey, coastal north-east Greenland, Polar Res., 35, https://doi.org/10.3402/polar.v35.21912, 2016.

Kobashi, T., Menviel, L., Jeltsch-Thömmes, A., Vinther, B. M., Box, J. E., Muscheler, R., Nakaegawa, T., Pfister, P. L., Döring, M., Leuenberger, M., Wanner, H., and Ohmura, A.: Volcanic influence on centennial to millennial Holocene Greenland temperature change, Sci. Rep., 7, 1–10, https://doi.org/10.1038/s41598-017-01451-7, 2017.

Kolling, H. M., Stein, R., Fahl, K., Perner, K., and Moros, M.: Short-term variability in late Holocene sea ice cover on the East Greenland Shelf and its driving mechanisms, Palaeogeogr. Palaeoclimatol. Palaeoecol., 485, 336–350, https://doi.org/10.1016/j.palaeo.2017.06.024, 2017.

Krieger, L., Floricioiu, D., and Neckel, N.: Drainage basin delineation for outlet glaciers of Northeast Greenland based on Sentinel-1 ice velocities and TanDEM-X elevations, Remote Sens. Environ., 237, 111483, https://doi.org/10.1016/j.rse.2019.111483, 2020.

Laberg, J. S., Forwick, M., and Husum, K.: New geophysical evidence for a revised maximum position of part of the NE sector of the Greenland ice sheet during the last glacial maximum, Arktos, 3, https://doi.org/10.1007/s41063-017-0029-4, 2017.

Lambeck, K., Rouby, H., Purcell, A., Sun, Y., and Sambridge, M.: Sea level and global ice volumes from the Last Glacial Maximum to the Holocene, Proc. Natl. Acad. Sci., 111, 15296–15303, https://doi.org/10.1073/pnas.1411762111, 2014.

Landvik, J. Y.: The last glaciation of Germania Land and adjacent areas, northeast Greenland, J. Quat. Sci., 9, 81–92, https://doi.org/10.1002/jqs.3390090108, 1994.

Lane, T. P., Roberts, D. H., Ó Cofaigh, C., Vieli, A., and Moreton, S. G.: The glacial history of the southern Svartenhuk Halvø, West Greenland, Arktos, 1, 1–28, https://doi.org/10.1007/s41063-015-0017-5, 2015.

Larsen, N. K., Funder, S., Linge, H., Möller, P., Schomacker, A., Fabel, D., Xu, S., and Kjær, K. H.: A Younger Dryas re-advance of local glaciers in north Greenland, Quat. Sci. Rev., 147, 47–58, https://doi.org/10.1016/j.quascirev.2015.10.036, 2016.

Larsen, N. K., Levy, L. B., Carlson, A. E., Buizert, C., Olsen, J., Strunk, A., Bjørk, A. A., and Skov, D. S.: Instability of the Northeast Greenland Ice Stream over the last 45,000 years, Nat.

1004   Commun., 9, 3–10, https://doi.org/10.1038/s41467-018-04312-7, 2018.

1005   Larsen, N. K., Søndergaard, A. S., Levy, L. B., Olsen, J., Strunk, A., Bjørk, A. A., and Skov, D.:
1006   Contrasting modes of deglaciation between fjords and inter-fjord areas in eastern North
1007   Greenland, Boreas, 49, 905–919, https://doi.org/10.1111/bor.12475, 2020.

1008   Larsen, N. K., Søndergaard, A. S., Levy, L. B., Strunk, A., Skov, D. S., Bjørk, A., Khan, S. A.,
1009   and Olsen, J.: Late glacial and Holocene glaciation history of North and Northeast Greenland,
1010   Arctic, Antarct. Alp. Res., 54, 294–313, https://doi.org/10.1080/15230430.2022.2094607, 2022.

1011   Lecavalier, B. S., Milne, G. A., Simpson, M. J. R., Wake, L., Huybrechts, P., Tarasov, L.,
1012   Kjeldsen, K. K., Funder, S., Long, A. J., Woodroffe, S., Dyke, A. S., and Larsen, N. K.: A model
1013   of Greenland Ice Sheet deglaciation constrained by observations of relative sea level and ice
1014   extent, Quat. Sci. Rev., 102, 54–84, 2014.

1015   Levy, L. B., Kelly, M. A., Lowell, T. V., Hall, B. L., Howley, J. A., and Smith, C. A.: Coeval
1016   fluctuations of the Greenland ice sheet and a local glacier, central East Greenland, during late
1017   glacial and early Holocene time, Geophys. Res. Lett., 43, 1623–1631, 2016.

1018   Lyså, A. and Vorren, T. O.: Seismic facies and architecture of ice-contact submarine fans in
1019   high-relief fjords, Troms, Northern Norway, Boreas, 26, 309–328, 1997.

1020   Mouginot, J., Rignot, E., Scheuchl, B., Fenty, I., Khazendar, A., Morlighem, M., Buzzi, A., and
1021   Paden, J.: Fast retreat of Zachariae Isstrom, Northeast Greenland, Science (80-.)., 350, 1357–
1022   1361, 2015.

1023   Mouginot, J., Bjørk, A. A., Millan, R., Scheuchl, B., and Rignot, E.: Insights on the Surge
1024   Behavior of Storstrømmen and L. Bistrup Bræ, Northeast Greenland, Over the Last Century,
1025   Geophys. Res. Lett., 45, 11,197-11,205, https://doi.org/10.1029/2018GL079052, 2018.

1026   Newton, A. M. W., Knutz, P. C., Huuse, M., Gannon, P., Brocklehurst, S. H., Clausen, O. R.,
1027   and Gong, Y.: Ice stream reorganization and glacial retreat on the northwest Greenland shelf,
1028   Geophys. Res. Lett., 44, 7826–7835, https://doi.org/10.1002/2017GL073690, 2017.

1029   Ó Cofaigh, C.: Flow Dynamics and till genesis associated with a marin-based Antarctic palaeo-
1030   ice stream, Quat. Sci. Rev., 24, 709–740, 2005.

1031   Ó Cofaigh, C., Dowdeswell, J. A., and Grobe, H.: Holocene glacimarine sedimentation, inner
1032   Scoresby Sund, East Greenland: The influence of fast-flowing ice-sheet outlet glaciers, Mar.
1033   Geol., 175, 103–129, https://doi.org/10.1016/S0025-3227(01)00117-7, 2001.

1034   Ó Cofaigh, C., Dowdeswell, J. A., Jennings, A. E., Hogan, K. A., Kilfeather, A., Hiemstra, J. F.,
1035   Noormets, R., Evans, J., McCarthy, D. J., Andrews, J. T., Lloyd, J. M., and Moros, M.: An
1036   extensive and dynamic ice sheet on the west greenland shelf during the last glacial cycle,
1037   Geology, 41, 219–222, https://doi.org/10.1130/G33759.1, 2013.

1038   Olsen, I. L., Forwick, M., Laberg, J. S., and Rydningen, T. A.: Last Glacial ice-sheet dynamics
1039   offshore NE Greenland – a case study from Store Koldewey Trough, The Cryosphere
1040   Discussions, 2020.

1041   Ottesen, D., Dowdeswell, J. A., and Rise, L.: Submarine landforms and the reconstruction of
1042   fast-flowing ice streams within a large Quaternary ice sheet: The 2500-km-long Norwegian-
1043   Svalbard margin (57°-80°N), Bull. Geol. Soc. Am., 117, 1033–1050,
1044   https://doi.org/10.1130/B25577.1, 2005.

1045   Ottesen, D., Dowdeswell, J. A., Benn, D. I., Kristensen, L., Christiansen, H. H., Christensen, O.,

Hansen, L., Lebesbye, E., Forwick, M., and Vorren, T. O.: Submarine landforms characteristic of glacier surges in two spitsbergen fjords, Quat. Sci. Rev., 27, 1583–1599, 2008.

Pados-Dibattista, T., Pearce, C., Detlef, H., Bendtsen, J., and Seidenkrantz, M. S.: Holocene palaeoceanography of the Northeast Greenland shelf, Clim. Past, 18, 103–127, https://doi.org/10.5194/cp-18-103-2022, 2022.

Pedersen, J. B. T., Kroon, A., and Jakobsen, B. H.: Holocene sea-level reconstruction in the Young Sound region, Northeast Greenland, J. Quat. Sci., 26(2), 219–226, 2011.

Rahmstorf, S., Box, J. E., Feulner, G., Mann, M. E., Robinson, A., Rutherford, S., and Schaffernicht, E. J.: Exceptional twentieth-century slowdown in Atlantic Ocean overturning circulation, Nat. Clim. Chang., 5, 475–480, https://doi.org/10.1038/nclimate2554, 2015.

Rasmussen, T. L., Pearce, C., Andresen, K. J., Nielsen, T., and Seidenkrantz, M.-S.: Northeast Greenland: ice-free shelf edge at 79.4°N around the Last Glacial Maximum 25.5–17.5 ka, Boreas, 51, 759–775, 2022.

Reeh, N., Bøggild, C. E., and Oerter, H.: Surge of Storstrømmen, a large outlet glacier from the Inland Ice of North-East Greenland, Rapp. Grønands Geol. Unders., 162, 201–209, 1994.

Reilly, B. T., Stoner, J. S., Mix, A. C., Walczak, M. H., Jennings, A., Jakobsson, M., Dyke, L., Glueder, A., Nicholls, K., Hogan, K. A., Mayer, L. A., Hatfield, Robert, G., Albert, S., Marcott, S., Fallon, S., and Cheseby, M.: Holocene break-up and reestablishment of the Petermann Ice Tongue, Northwest Greenland, Quat. Sci. Rev., 218, 322–342, 2019.

Reimer, P. J., Austin, W. E. N., Bard, E., Bayliss, A., Blackwell, P. G., Bronk Ramsey, C., Butzin, M., Cheng, H., Edwards, R. L., Friedrich, M., Grootes, P. M., Guilderson, T. P., Hajdas, I., Heaton, T. J., Hogg, A. G., Hughen, K. A., Kromer, B., Manning, S. W., Muscheler, R., Palmer, J. G., Pearson, C., Van Der Plicht, J., Reimer, R. W., Richards, D. A., Scott, E. M., Southon, J. R., Turney, C. S. M., Wacker, L., Adolphi, F., Büntgen, U., Capano, M., Fahrni, S. M., Fogtmann-Schulz, A., Friedrich, R., Köhler, P., Kudsk, S., Miyake, F., Olsen, J., Reinig, F., Sakamoto, M., Sookdeo, A., and Talamo, S.: The IntCal20 Northern Hemisphere Radiocarbon Age Calibration Curve (0-55 cal kBP), Radiocarbon, 62, 725–757, https://doi.org/10.1017/RDC.2020.41, 2020.

Rignot, E., Bjork, A., Chauche, N., and Klaucke, I.: Storstrømmen and L. Bistrup Bræ, North Greenland, Protected From Warm Atlantic Ocean Waters, Geophys. Res. Lett., 49, https://doi.org/10.1029/2021GL097320, 2022.

Rydningen, T. A., Vorren, T. O., Laberg, J. S., and Kolstad, V.: The marine-based NW Fennoscandian ice sheet: Glacial and deglacial dynamics as reconstructed from submarine landforms, Quat. Sci. Rev., 68, 126–141, https://doi.org/10.1016/j.quascirev.2013.02.013, 2013.

Sættem, J.: Glaciotectonic forms and structures on the Norwegian continental shelf: observations, processes and implications, Nor. Geol. Tidsskr., 70, 81–94, 1990.

Schaffer, J., von Appen, W.-J., Dodd, P. A., Hofstede, C., Mayer, C., de Steur, L., and Kanzow, T.: Warm water pathways toward Nioghalvfjerdsfjorden Glacier, Northeast Greenland, J. Geophys. Res. Ocean., 122, 4004–4020, https://doi.org/10.1002/2016JC012462.Received, 2017.

Schmidt, S., Wagner, B., Heiri, O., Klug, M., Bennike, O., and Melles, M.: Chironomids as indicators of the Holocene climatic and environmental history of two lakes in Northeast Greenland, Boreas, 40, 116–130, https://doi.org/10.1111/j.1502-3885.2010.00173.x, 2011.

Schoof, C. G. and Clarke, G. K. C.: A model for spiral flows in basal ice and the formation of subglacial flutes based on a Reiner-Rivlin rheology for glacial ice, J. Geophys. Res. Solid Earth, 113, 1–12, https://doi.org/10.1029/2007JB004957, 2008.

Shaw, J., Pugin, A., and Young, R. R.: A meltwater origin for Antarctic shelf bedforms with special attention to megalineations, Geomorphology, 102, 364–375, https://doi.org/10.1016/j.geomorph.2008.04.005, 2008.

Shreve, R. L.: Esker characteristics in terms of glacier physics, Katahdin esker system, Maine., Geol. Soc. Am. Bull., 96, 639–646, https://doi.org/10.1130/0016-7606(1985)96<639:ECITOG>2.0.CO;2, 1985.

Skov, D. S., Andersen, J. L., Olsen, J., Jacobsen, B. H., Knudsen, M. F., Jansen, J. D., Larsen, N. K., and Egholm, D. L.: Constraints from cosmogenic nuclides on the glaciation and erosion history of Dove Bugt , northeast Greenland, GSA Bull., 1–13, 2020.

Slabon, P., Dorschel, B., Jokat, W., Myklebust, R., Hebbeln, D., and Gebhardt, C.: Greenland ice sheet retreat history in the northeast Baffin Bay based on high-resolution bathymetry, Quat. Sci. Rev., 154, 182–198, https://doi.org/10.1016/j.quascirev.2016.10.022, 2016.

Smith, L. M. and Andrews, J. T.: Sediment characteristics in iceberg dominated fjords, Kangerlussuaq region, East Greenland, Sediment. Geol., 130, 11–25, https://doi.org/10.1016/S0037-0738(99)00088-3, 2000.

Stacey, C. D. and Hill, P. R.: Cyclic steps on a glacifluvial delta, Howe Sound, British Columbia, in: Atlas of Submarine Glacial Landforms: Modern, Quaternary and Ancient, edited by: Dowdeswell, J. A., Canals, M., Jakobsson, M., Todd, B. J., Dowdeswell, E. K. & Hogan, K. A., Geological Society of London, 93–94, 2016.

Stocker, T. F., Qin, D., Plattner, G.-K., Tignor, M. M. B., Allen, S. K., Boschung, J., Nauels, A., Xia, Y., Bex, V., and Midgley, P. M.: Climate Change 2013: The Physical Science Basis. Contribution of Working Group I to the Fifth Assessment Report of the Intergovernmental Panel on Climate Change, Cambridge, 2013.

Stokes, C. R. and Clark, C. D.: Geomorphological criteria for identifying Pleistocene ice streams, Ann. Glaciol., 28, 67–74, https://doi.org/10.3189/172756499781821625, 1999.

Stokes, C. R. and Clark, C. D.: Palaeo-ice streams, Quat. Sci. Rev., 20, 1437–1457, 2001.

Storrar, R. D., Stokes, C. R., and Evans, D. J. A.: Morphometry and pattern of a large sample (>20,000) of Canadian eskers and implications for subglacial drainage beneath ice sheets, Quat. Sci. Rev., 105, 1–25, https://doi.org/10.1016/j.quascirev.2014.09.013, 2014.

Syring, N., Lloyd, J. M., Stein, R., Fahl, K., Roberts, D. H., Callard, L., and O'Cofaigh, C.: Holocene interactions between glacier retreat, sea ice formation, and Atlantic water advection at the inner Northeast Greenland continental shelf, Paleoceanogr. Paleoclimatology, 35, 2020.

Wagner, B., Bennike, O., Bos, J. A. A., Cremer, H., Lotter, A. F., and Melles, M.: A multidisciplinary study of Holocene sediment records from Hjort Sø on Store Koldewey, Northeast Greenland, J. Paleolimnol., 39, 381–398, https://doi.org/10.1007/s10933-007-9120-3, 2008.

Weber, M. E., Niessen, F., Kuhn, G., and Wiedicke, M.: Calibration and application of marine sedimentary physical properties using a mult-sensor core logger, Mar. Geol., 136, 151–172, 1997.

1131 Weidick, A., Andreasen, C., Oerter, H., and Reeh, N.: Neoglacial glacier changes around
1132 Storstrommen, north-east Greenland, Polarforschung, 64, 95–108, 1994.

1133 Wilson, N. J. and Straneo, F.: Water exchange between the continental shelf and the cavity
1134 beneath Nioghalvfjerdsbræ (79 North Glacier), Geophys. Res. Lett., 42, 7648–7654,
1135 https://doi.org/10.1002/2015GL064944, 2015.

1136 Winkelmann, D., Jokat, W., Jensen, L., and Schenke, H. W.: Submarine end moraines on the
1137 continental shelf off NE Greenland - Implications for Lateglacial dynamics, Quat. Sci. Rev., 29,
1138 1069–1077, https://doi.org/10.1016/j.quascirev.2010.02.002, 2010.

1139